International Journal of Innovation Engineering and Science Research

Editorial Board

International Journal of Innovation Engineering and Science Research

Volume 2 ISSUE 3 May-June 2018

International Journal of Innovation Engineering and Science Research

Open Access

Probabilistic Polling System Approach for IoT Secure Routing

Seyed Mahmood Hashemi
Beijing University of Technology
Beijing, CHINA

ABSTRACT

The Internet of things (IoT) affects on humans life deeply. There are traditional cyber threats and also new threats. There is no guard and immunity for systems against the innumerable variance of attack and exploitation. In this paper, an approach base on Polling System is presented for secure routing IoT devices. We use polling system with probabilistic routing, so there is a probability to move from one queue to another. Probabilistic polling system allows us to perform priority of stakeholders' votes.

Keywords- *Internet of Things; Secure Routing; Polling System*

I. INTRODUCTION

The Internet of things (IoT) affects on humans life deeply [9]. Although the new IoT functionality of smart devices causes to the better life for the human, there are traditional cyber threats and also new threats. However there were many works on the IoT security, most of them were not Use-Centric. In against of the previous works, the proposed approach is base on the interaction with users, so it is User-Centric completely. In a broad view, we divide IoT networks into two categories: 1- consumer and 2- industrial. While we use IoT devices in a smart home, we emphasize on the smart point of the IoT devices. In other words, the ideal point of IoT devices is communicated and adjusting to other physical devices in the home. While a set of smart home devices has a particular behavior or need for special decision making, we called them as user-centric IoT (UCIoT) [10].

There is no guard and immunity for systems against the innumerable variance of attack and exploitation. Thus security mechanism has fought to keep with IoT. Intelligence is successful to detect the intruder. IoT has the challenge to bridge physical with the cyber world [11]. Previous security mechanisms must be adapted in order to maintain defensive expectation.

In this paper, an approach base on Polling System is presented for secure routing IoT devices. In the classical view, Polling System is a set of one server and multiple queues. Clients are arrived and set into queues and then get server according to a particular policy. (figure 1)

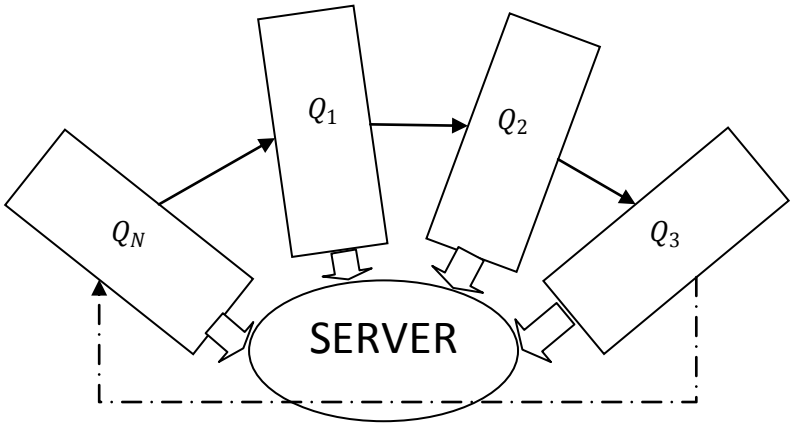

Fig. 1. Classical Polling System

The number of queues and also the capacity of queues are predefined. In the beginning, Polling System is used for the time-sharing computer system, but now it is used to model wide variety applications (computer communications, robotics, traffic and transportation, manufacturing, production, mail distribution, etc.) [12, 13, 14]. In the time-sharing polling system, there are N terminals that are connected to a central computer. The central computer visit terminals in turn and cyclic order. The size of queues is finite and the arrival process is independent Poisson Process with parameter λ_i.

Several service policies are examined on the basic model of Polling System such as exhaustive, gated, and limited-I policies. The server policy determines association server to clients. The basic Polling model can be applied in different applications: Token Ring Networks; Robotic Systems; Various Non-Generic Computers; Communication Systems. The common scheme for Polling System is a server resource shared by multiple queues. The basic model of Polling System is cyclic polling model. In the next step, the fixed polling order is replaced with random polling order. The important measure of the performance of Polling System is Response Time [15, 16]. In the Polling System with probabilistic routing, when the client in queue i is serviced, it is routed to queue j with probability$p_{i,j}$.

In this paper, we use polling system with probabilistic routing. Polling system provides a platform for security voting of all stakeholders. In the other side, probabilistic routing establishes priority approach. Therefore the presented approach can be used in the organization with employees by different priority.

This paper is organized as follow: section 2 is the study of related works; section 3 explains proposal algorithm, finally, section 4 is the conclusion.

II. Related Works

Akatyev et. Al. assume heterogeneous IoT devices. they use data flow diagram to represent the dependencies between users and information [1, 20]. In [2, 21, 22], In this survey, authors categorize IoT security issues into three groups: 1- low-level security issues; 2- intermediate-level security issues and high-level security issues and then study about security mechanism for each of them. Coulter et. al. research in current intrusion detection approaches from an intelligence perspective.

Levy et. al.define different types of polling systems [4, 23, 24]. Time-sharing polling system, there are N terminals that are connected to a central computer. The central computer visit terminals in turn and cyclic order. The size of queues is finite and the arrival process is independent Poisson Process with parameter λ_i. In [5], Authors use a $M/M/1$ queue to model the traffic of the network. Yang et. al. propose an approach to estimate the mean queue length, mean cycle time and throughout for two-class priority-based polling system. Tags energy conservation is the top priority in RFID systems.In a

typical RFID, which has one or multiple readers and numerous tags, each tag (carrier identifier) is communicated directly to readers. Tags, base on battery consumption, are divided into two groups: 1- active and 2- passive. Passive tags do not have an internal battery and instead of it, they are used radio waves. While there are many warehouse products whit own tags, passive tags cause to interference and sophisticated communication. Active tags against passive tags have own battery-powered and can be used in mobile status. [7] presents an approach to design an efficient protocol for active tags. Cyber-Physical Systems (CPS) are set of different devices include computational, networked, communicational and sensor devices [8, 18, 19]. CPS can be used for monitor, control and in general wireless communication. CPS architecture has three layers: 1- Cyber layer, 2- physical layer and 3- Networking layer.

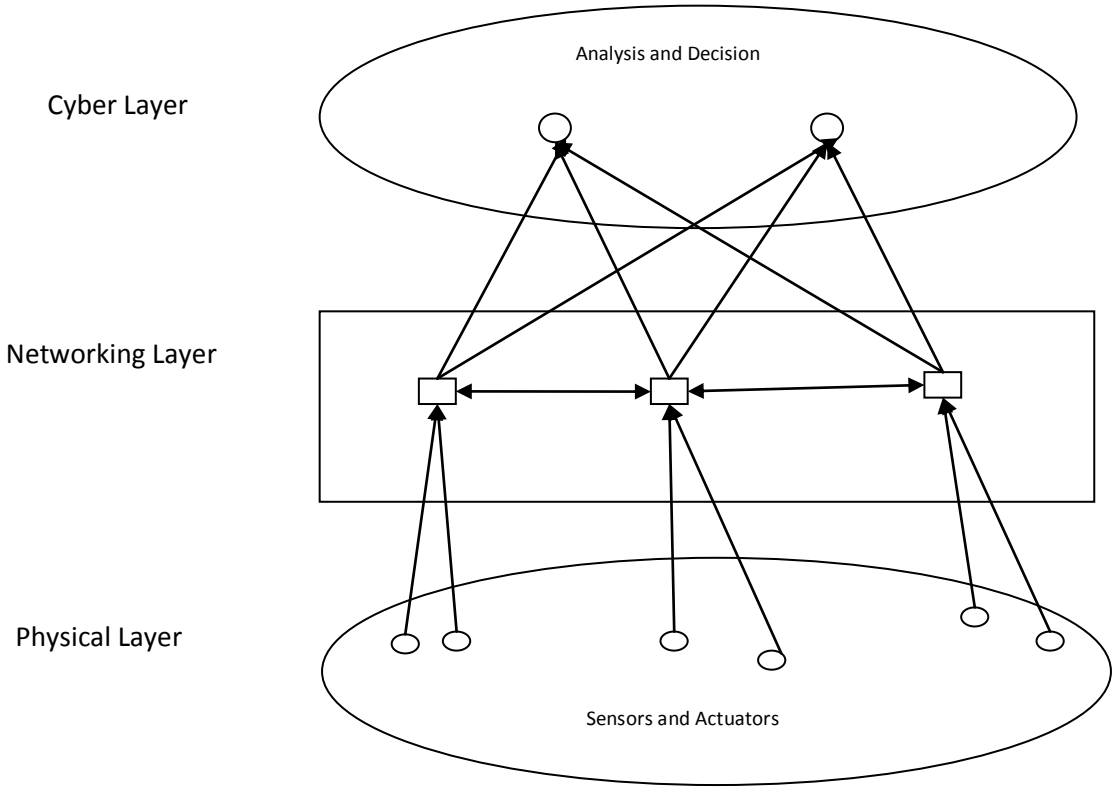

Fig. 2. Security Levels

Since inefficient utilization of bandwidth, deterministic Multi-Access Control (MAC) protocols are not adapted to the requirements of CPS. In a polling MAC protocol, request to transmit data packets are done base on the density of in polling list. Zheng et. al. design a polling MAC protocol to meet the requirements of CPS applications. In that protocol, authors use Orthogonal Frequency Division Multiplexing (OFDM), which is the contention of IEEE 802.11 [8, 16].

Previous works specified two points: 1-using polling system to gather different opinions and 2-apply priority in polling system to different users.

III. 3 Proposed Algorithm

The data packets need to route while they are transferred via the network. There are different parameters to select a suitable path. In the other side, there are different stakeholders that have opinions to transfer a data packet. In the simplest situation, there is SERVER on the one side and there is CLIENT on the other side. The most route approaches concern some special formulas. Although their approach is common and usable, the users' opinions are ignored. Proposed algorithm concerns

users' opinions, indeed it considers the priority of stakeholders. Actually, all stakeholders do not have same expertise, so there must be a difference between stakeholders.

In this paper, users decide about a suitable path. The users take their opinions about the feasible paths (as votes) and then the suitable path is decided base on votes. In the proposed algorithm, there is a queue for voting users. Users can give their vote in this queue, and also their position can rise to the next queue according to the following probability:

$$p = a_n/(a_1 + \cdots + a_m)$$
(1

While $a_1 + \cdots + a_m$ are coefficients of queues and set as default. a means coefficient of nth queue. Coefficients are sorted ascend to descend, so the probability to raise positions of stakeholders reduces in each epoch of algorithm.

Above probability is used just when there is no pre-knowledge of stakeholders, but if there is pre-knowledge for priority of stakeholders, it can be applied without probability. When all stakeholders are assigned in queues, the final vote is calculated by adding votes in different queues multiply their coefficients.

Let assign coefficients as follow:

$$a = [8\ 6\ 5\ 4]$$
(2

There are 20 stakeholders in the system and four queues, so the probability of queues are as:

$$p_1 = 0.34, p_2 = 0.26, p_3 = 0.21\ p_4 = 0.21$$
(3

IV. 4 Conclusion

In this paper, an approach base on Polling System is presented for secure routing IoT devices. Polling System is used because one important parameter for secure routing is stakeholders' opinions. Since there is a difference between the positions of stakeholders, we use probabilistic polling system. In presented system, clients in queues are visited (voting policy) according to a probability. Actually, we can change the voting policy or set some clients as constant in some queues. There is need to pre-knowledge to set the constant position of clients, but there is an opportunity for this job in the paper.

References

[1] Nikolay Akatyev, Joshua I. James, "Evidence identification in IoT networks based on threat assessment", ELSEVIER, Future Generation Computer Systems.

[2] Minhaj Ahmad Khan, Khaled Salah, "IoT security: Review, block chain solutions, and open challenges", ELSEVIER, Future Generation Computer Systems.

[3] Rory Coulter, Lei Pan, "Intelligent agents defending for an IoT world: A review", ELSEVIER, computers & s e c u r i t y 73 (2 0 1 8) 439–458

[4] HANOCH LEVY, MOSHE SIDI, "Polling Systems : Applications, Modeling, and Optimization", IEEE TRANSACTIONS ON COMMUNICATIONS. VOL. 38, NO. 10, OCTOBER 1990

[5] JIANG Wei, TIAN Zhihong, CAI Chao, GONG Bei, "Bottleneck Analysis for Data Acquisition in High-Speed Network Traffic Monitoring", NETWORK TECHNOLOGY AND APPLICATION

[6] Zhijun Yang, Hongwei Ding, "Characteristics of a Two-Class Polling System Model", TSINGHUA SCIENCE AND TECHNOLOGY, ISSNll1007-0214ll11/13llpp516-520, Volume 19, Number 5, October 2014

[7] Yan Qiao, Shigang Chen, Tao Li, Shiping Chen, "Tag-Ordering Polling Protocols in RFID Systems", IEEE/ACM TRANSACTIONS ON NETWORKING, VOL. 24, NO. 3, JUNE 2016

[8] Meng Zheng, Junru Lin, Wei Liang, Haibin Yu, "A Priority-aware Frequency Domain Polling MAC Protocol for OFDMA-based Networks in Cyber-physical Systems", IEEE/CAA JOURNAL OF AUTOMATICA SINICA, VOL. 2, NO. 4, OCTOBER 2015

[9] Anita Vorster, Les Labschagne, "A Framework for Comparing Different Information Security Risk Analysis Methodologies", ACM, Proceeding of SAICSIT 2005, pp. 95-103

[10] Jakub Breier, Ladislav Hudec, "Risk Analysis Supported by Information Security Metrics", ACM, International Conference on Computer Systems and Technologies, CompSysTech'11, 2011

[11] Januszkiewicz Paulina, Pyka Marek, "Designing a Security Policy According to BS 7799 Using the OCTAVE Methodology", IEEE, Second International Conference on Availability, Reliability and Security (ARES'07), 2007

[12] Johannes Viehmann, "Reusing Risk Analysis Results, An Extension for the CORAS Risk Analysis Method", IEEE, International Conference on Social Computing, 2012

[13] Li-Xin Wang, "a course in fuzzy system and control", Prentice-Hall International, Inc., pp. 4-7, 1997

[14] Nan Feng, Harry Jinnan Wang, Minqiang Li, "A security risk analysis model for information system: Casual relationships of risk factors and vulnerability propagation analysis", ELSEVIER, Information Sciences 256 (2014) 57-73

[15] Maisa Mendonca Silva, Ana Paula Henriques de Gusmão, Thiago Poleto, Lúcio Camara e Silva, Ana Paula Cabral Seixas Costa, "A multidimensional approach to information security riskmanagement using FMEA and fuzzy theory", ELSEVIER, International Journal of Information Management 34 (2014) 733–740

[16] L. Klienrock, H. Levy, "the analysis of random polling systems", Operation Research Society of America, 1998

[17] A. Wierman, E. M. M. Winands, O. J. Boxama, "scheduling in polling systems", ELSEVIER, 2007

[18] W. Bux, "local-area subnetworks: a performance comparison", IEEE, Transaction on Communications, 29(10):1465-1473, 1981

[19] T. Li, D. Logothetis, M. Veeraraghavan, "analysis of a polling system for telephony traffic with application to wireless LANs", IEEE, transaction on wireless communications, Vol. 5, No. 6, 2006

[20] J. A. Weststrate, "analysis and optimization of polling systems", PhD thesis, Tilburg University, 1992

[21] D. Gupta, M. M. Srinivasan, "polling systems with state-independent setup times", Queueing Systems, 22:403-423, 1996

[22] J. A. Weststrate, "analysis and optimization of polling systems", PhD thesis, Tilburg University, 1992

[23] A. Federgruen, Z. Katalan, "costumer waiting-time distributions under base-stock policies in single facility multi-item production systems", Naval Research Logistics, 43:533-548, 1996

[24] A. Federgruen, Z. Katalan, "the stochastic economic lot scheduling problem: cyclical base-stock policies with idle times", Management Science, 44:989-1001, 1996

International Journal of Innovation Engineering and Science Research

Open Access

Subsistence of Host Guest Inclusion Complexes ofBiologically Active Moleculeswith Ionic Liquid Probed by Physicochemical Exploration

KalipadaSarkar[$], Niloy Roy[#],Raja Ghosh[#], MahendraNath Roy*

[$] *Assistant Professor, Department of Chemistry, Islampur College, Islampur, Uttar Dinajpur, India,*
[#]*Department of Chemistry, University of North Bengal, Darjeeling*
* *Professor and Corresponding Author, Department of Chemistry, University of North Bengal, Darjeeling, India*

ABSTRACT

In this present work we studied the supramolecular interaction of 1-hexyl-3-methylimidazolium hexaflurophosphate(HMIm)$PF_6$with α-cyclodextrin (α-CD) and β-cyclodextrin (β-CD) using various physicochemical method and spectroscopic technique. The formation of inclusion complex of any ionic liquid inside the cyclodextrin affects the physicalchemical properties like solubility, conductivity, surface tension, etc. So from the discrepancy of physicochemical andspectral properties we can confirm the formation inclusion complex. The stoichiometry of host - guest of the inclusion complexes was evaluated from conductivity, surface tensionstudy and Job's plot from UV-visible spectroscopy. We also calculated the association/binding constant from conductivity, surface tension measurements and Benesi-Hildebrand equation. The infra-red (IR) and ^{1}H NMR spectroscopy also affirm the formation of inclusion complexes however the plausible mode of inclusion was described from ^{1}H NMR and 2D ROESY NMR spectroscopies.

Key words: Inclusion complex, cyclodextrins, Benesi-Hildebrand equation, 1-hexyl-3-methylimidazolium hexaflurophosphate,

I. Introduction

The cyclodextrins(CDs) are the truncated shaped cyclic oligosaccharides having n glucopyranose units. The three kinds of cyclodextrins namely α -cyclodextrin (α-CD), β -cyclodextrin(-CD) and γ-cyclodextrin(γ-CD) contain 6, 7 and 8 glucopyranose units respectively which are attached together by α-(1–4) linkages [1,2].The structure of cyclodextrins are shown in **Scheme1** and **2**. The inner cavity of cyclodextrin is hydrophobic in nature whereas exterior part is hydrophilic in nature. This kind of unique features make cyclodextrin suitable for complexion with different kind of molecules like vitamins, amino acids, ionic liquids, hormones, polymers,dyes etc. [3-7]. The hydrophobic parts of the ionic liquid become encapsulated inside the hydrophobic cavity of cyclodextrins and thus forming a stable inclusion complex [8].

The formation of inclusion complexes increase the solubility, stability against heat, light, oxidation and bioavailability andreduce volatility of the guest moleculeswithout disturbing the structure of host molecules.

3D View of cyclodextrin

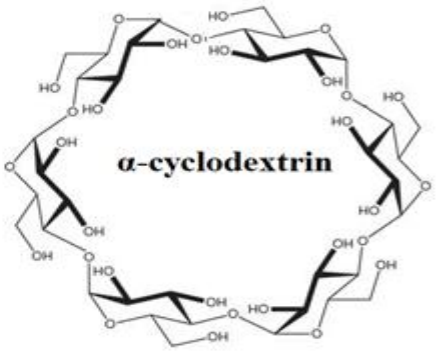

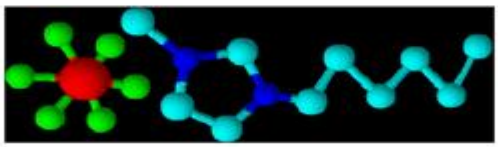

1-hexyl-3-methylimidazolium hexaflurophosphate

Scheme 1: Structure of cyclodextrin and 1-hexyl-3-methylimidazolium hexaflurophosphate

Ionic liquids (ILs) have some special properties such as non-flammability, chemical and thermal stability, high polarity, non-volatility and non-hazardous character [9, 10]. Ionic liquids (ILs) are extensively used in variousarenas of chemistry like electrochemistry, supramolecular chemistry, nuclear chemistry, industrial chemistry etc. [11, 12]. It is also used in processing of cellulose, chemical syntheses, recycling of waste materials, electrophoresis and high-performance liquid chromatography[13, 14]. Due to the non-hazardous feature, ionic liquids are considered as green solvents in various organic and inorganic reactions.

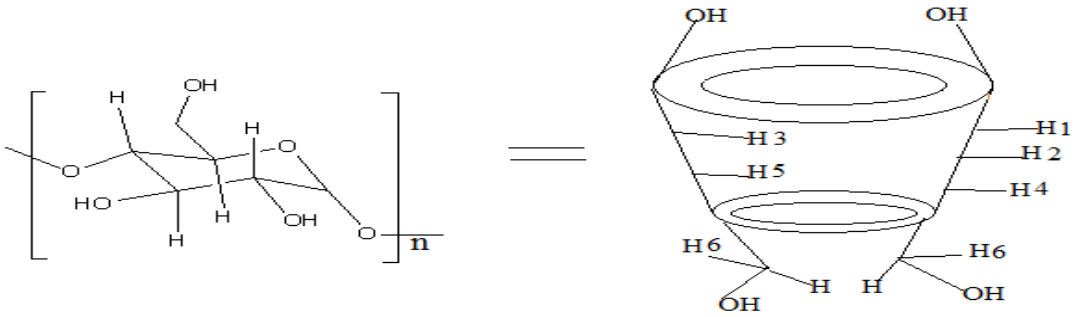

Scheme-2: Structure of cyclodextrin

The studied ionic liquid, 1-hexyl-3-methylimidazolium hexaflurophosphate(HMIm)PF_6acts as a cationic surfactant and forms inclusion complex with cyclodextrins. In this article we studied the formation of self-assembly inclusion complex of this ionic liquid inside the cavity of α- and β- cyclodextrins. Various physicochemical and spectrometric methods were used to examine the inclusion phenomenon. The inclusion complexes so formed may be applied in agriculture textile, detergent, food, the drug or pharmaceutical and cosmetics as antistatic, corrosion inhibitory, antibacterial, emulsifying, dispersants, solubilizing agents etc.

II. Experimental Section

2.1. Materials

The IL, 1-hexyl-3-methylimidazolium hexaflurophosphate(HMIm)PF_6 was procured from TCI Chemicals (Japan) Pvt. Ltd and α -and β- cyclodextrins were procured from Sigma-Aldrich, Germany. All these chemicals were used as purchased as their mass fraction purity were >0.98.

2.2 Apparatus and procedure

Triply distilled water was taken to prepare the solutions. The weight was taken on an electronic balance, Mettler AG-285 accuracy of which was ±0.0003 x 10-3 kg.

The surface tensions (γ) of the solutions of the studied IL with varying concentration of cyclodextrins were measured with tensiometer (K9, KRUSS; Germany). Carefully washed platinum plate was used for measuring the surface tension after calibrating the tensiometerwith Millipore water [15]

The conductances of ionic liquid solutions in presence of varying concentrations of cyclodextrins were taken with Systronic-308 conductivity meter comprised with dip-type conductivity cell. The cell constant was calibrated with aqueous KCl (0.01M and 0.1M) solution [16]. The cell constant is approximately 0.1 ± 0.001 cm^{-1}. The solution of CDs was added with micro-pipette keeping the solution in a thermostat. The conductance was recorded when the solution reached in the equilibrium temperature.

UV-vis absorption spectra of varying concentration of ionic liquid and CDs were taken at 298.15 K by JASCO V-530 UV-VIS Spectrophotometer. Since the studied ionic liquid does not absorb in the UV and VIS range, we used methyl orange (MO) as a probe.

The FT-IR spectra of the solutions were takenfrom Perkin Elmer FT-IR spectrometer after preparing the KBr disk of IL, CDs and inclusion complexes. The KBr disk wasprepared by mixing 100 mg of the KBr and 1 mg of the compound thoroughly.

^{1}H NMR, NMR-ROSEY spectra was taken at 298 K in D_2O by BrukerAvance400 MHz spectrometer.

III. Result and discussion

3.1. Surface tension study

The surface tension study provides an important clue about the formation of inclusion complexes of cyclodextrins with any guest molecule [17, 18]. No any notable variation of surface tension occurs on addition CDs in water which indicates thatα-and β- cyclodextrins are surface inactive compounds [19]. But when we measured the surface tension of ionic liquid solution with successive addition of cyclodextrin solution, wewitnessed that the surface tension values increase with the increasing concentration of the cyclodextrin up to a certain level after which the surface tension values diminish gradually**(Fig.1).**The values of surface tension corresponding to the end-point of different mixtures are reported in **Table.1**. This trend may be regarded as the development of bigger micelle and the process goes on up to a certain concentration of CD which may be described on the basis of the formation of inclusion complexes (**Scheme 3**). The alkyl part of the ionic liquid becomes encapsulated into the cavity of CDs due to the existence of hydrophobic –hydrophobic interaction and the ionic part of the ionic liquid left outside the cavity of CD. It is also observed in the plot of surface tension vs. molarity of CDs that there is asingle break point which specifies that the stoichiometry of inclusion complex is 1:1. More break points will indicate 1:2 or 2:1stoichiometry (**Scheme 4**)

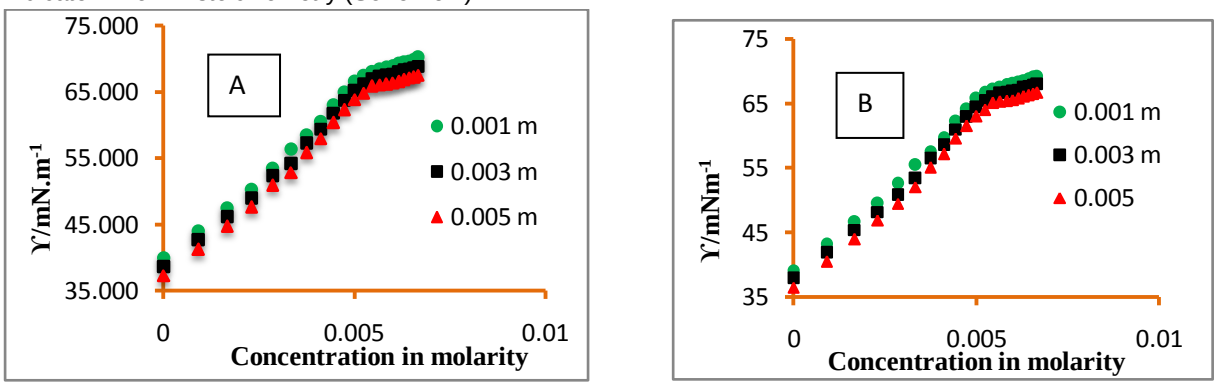

Fig.1. Variation of surface tension of (HMIm)PF_6 with the added conc. of aq
(A) α -cyclodextrin and (B) β-cyclodextrin.

Table 1.

Surface tension valuesat the break point in different mass fractions of aqueous cyclodextrins at 298.15 K

Molarity of IL	Surface tension at break point for β-CD **Ɣ/mN.m^{-1}**	Surface tension at break point for α-CD **Ɣ/mN.m^{-1}**
0.001 m	63.83	63.05
0.003 m	65.25	64.46
0.005 m	66.6	65.85

Association constants of 1:1 inclusion complexes (ICs) may be derived from the surface tension measurements using the following equation.

We can also derive the association constants for 1:1 inclusion complexes from surface tension measurements using the following quantitative relation [20].

CD + S = CDS (1)

$K_a = \frac{[CDS]}{[CD][S]}$ (2)

$CD_0 = [CD] + [CDS]$ (3)

$S_0 = [S] + [CDS]$ (4)

Where K_a = association constant, S = ionic liquid, CDS = inclusion complex, CD_0= total concentration of cyclodextrin and S_0=total concentration of IL.

$K_a = \frac{S_0 - [S]}{(CD_0 - S_0 + [S])[S]}$ (5)

$\frac{1}{K_a} = \frac{(CD_0 - S_0 + [S])[S]}{S_0 - [S]} = \frac{(CD_0 - S_0 + [S])}{\frac{S_0}{[S]} - 1}$ (6)

$S_0 - [S] = -\frac{1}{K_a}\left(\frac{S_0}{[S]} - 1\right) + CD_0$ (7)

The (S_0 – [S]) varies linearly with ($\frac{S_0}{[S]} - 1$). If we draw a plot of (S_0 – [S]) vs. ($\frac{S_0}{[S]} - 1$), we will get a straight line with the slope 1/K_a and intercept CD_0 **(Fig.2**). So association constant of formation of inclusion complexes = 1/slope. The association constants calculated in this method for OMImBr/ α-CD system is 1.23x103M^{-1}and for OMImBr/ β-CD system is1.34x103M^{-1}.

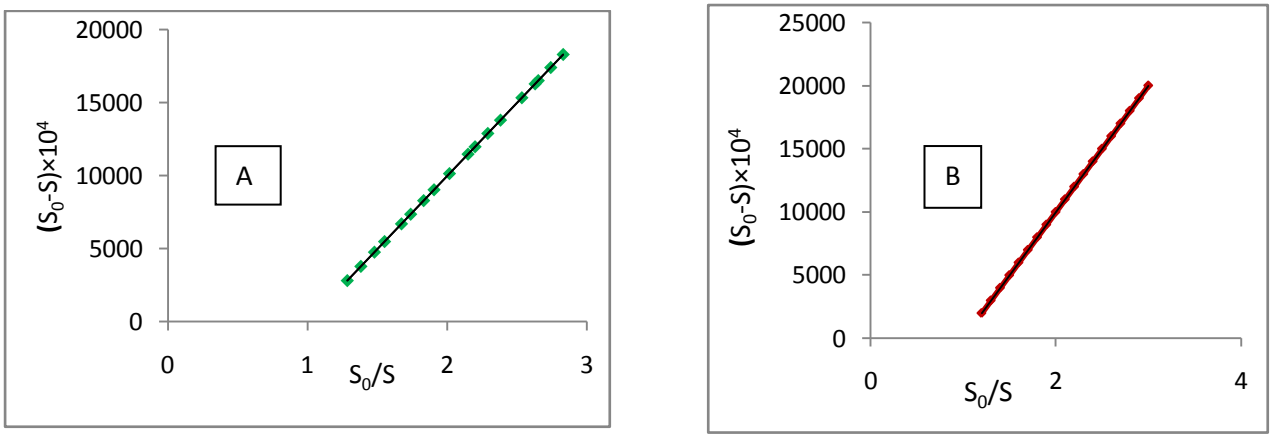

Fig.2. Plot of (S_0– [S]) against (S_0/[S]-1) for (A) $(HMIm)PF_6$ / α-cyclodextrin system (B) $(HMIm)PF_6$ /β-cyclodextrin system

3.2 Conductivity study

Theformation of inclusion complexescan also be described by conductivity study with more precision[21, 22]. The conductivities of the ionic liquid solutionswere measured with successive addition of CD solutions at 298.15 K.

The variations of conductance with molarity of α- and β-cyclodextrins are shown in **Fig.3**. It is seen that the values of conductance decrease gradually with molarities of CDs up to a certain point after which the conductance become steady. The molar conductance values corresponding to the end-point of different mixtures are given in **Table 2.**This incidence can be explained on the basis of formation ofhost and guest inclusion complexes. The hydrophobic alkyl part of (HMIm)PF_6enters into the cavity of α- and β-cyclodextrins and forminclusion complexes. The mobility of the IL decreases due to penetration of the IL inside the cavity of CDs as a result the conductance values decrease gradually with the concentration of CDs. The concentration of (HMIm)$PF_6$and cyclodextrin at the break point of the conductance vs. [CD] graph which suggests the formation 1:1 stoichiometric inclusion complexes[23, 24].

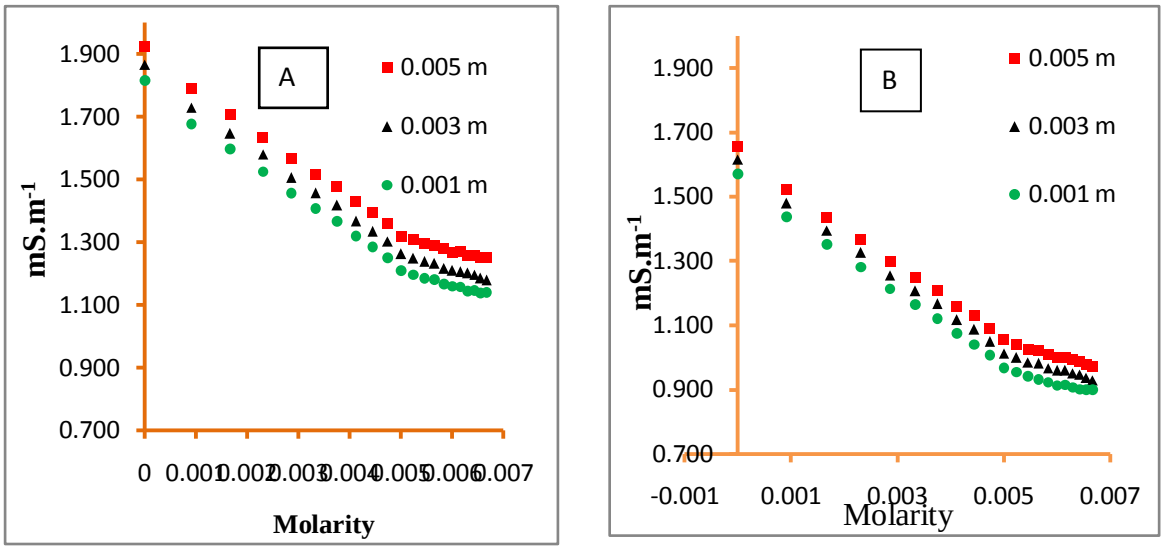

Fig.3. Variation of conductance of (HMIm)PF_6 with the added concentration of aqueous (A) α-cyclodextrin and (B) β-cyclodextrin

Table 2.

Values of conductance at the break point in different mass fractions of aqueous cyclodextrins at 298.15 K

Molarity of IL	Conductance at break point for β-CD **mS.m^{-1}**	Conductance at break point for α-CD **mS.m^{-1}**
0.001 m	1.21	0.968
0.003 m	1.263	1.013
0.005 m	1.32	1.055

The association constant of the 1:1 inclusion complexes of ionic liquid/cyclodextrin system can be evaluated by the non-linear programme at varying temperatures as follows[25, 26].

$IL_f + CD_f = IC$ (8)

The association constant (K_a) of inclusion complex may be expressed as

$$K_a=\frac{[IC]}{[IL]_f\times[CD]_f} \quad (9)$$

where, [IC] is the concentration of inclusion complex, $[IL]_f$ is the concentration of free ionic liquids and and $[CD]_f$is the concentration offree cyclodextrin respectively. As per the binding isotherm, the association constant (K_a) of the formation of inclusion complex may be written as

$$K_a = \frac{(K_{obs}-K_0)}{(K-K_{obs})\times[CD]_f} \quad (10)$$

$$[CD]_f = [CD]_{ad} - \frac{[IL]_{ad}-(K_{obs}-K_0)}{K-K_0} \quad (11)$$

Here, K_o, K_{obs} and K symbolize the conductance of (IL + CD) mixtures at initial, during the addition of CD and final state respectively.
Here, Ko, Kobs and K are the conductance of IL + CD mixture at starting, during the addition of CD and final state respectively and $[IL]_{ad}$ and $[CD]_{ad}$symbolize the concentrations of the added IL and added CD respectively. We can deriveK_a from the above equations (10) and (11) using the value of $[CD]_f$.The larger K_a value for β-CD than α-CD signifies that the former fits better than the later.
The thermodynamic parameters like enthalpy, entropy and free energy for the formation of the inclusion complex of $(HMIm)PF_6$into cyclodextrins can be evaluated as follows.

$$2.303\log Ka = -\frac{\Delta H_0}{RT} + \frac{\Delta S_0}{R} \qquad (12)$$

The plot of $\log K_a$against 1/T gives a straight line with an intercept $\Delta S_0/2.303R$ and a slope of $\Delta H_0/2.303R$. So from the value of intercept and slope we can easily calculate ΔS_0 and ΔH_0 and also ΔG of the formation of the inclusion complexes (reported in the **Table 1**). The negativeΔGvalues signify the spontaneityof the process[27, 28].

Table 1.

Association constants (K_a), Gibb's free energy, enthalpy and entropy of ionic liquid/cyclodextrin systems

IL and CD system	logKa (M^{-1})			ΔG (kJ mol^{-1})	ΔH (kJ mol^{-1})	ΔS (J mol-1) K^{-1}
	293.15 K	303.15 K	313.15 K			
OMImBR and α-CD	3.078	2.93	2.81	-29.882	-23.570	-21.53
OMImBR and β-CD	3.187	3.023	2.94	-25.545	-21.674	-13.2058

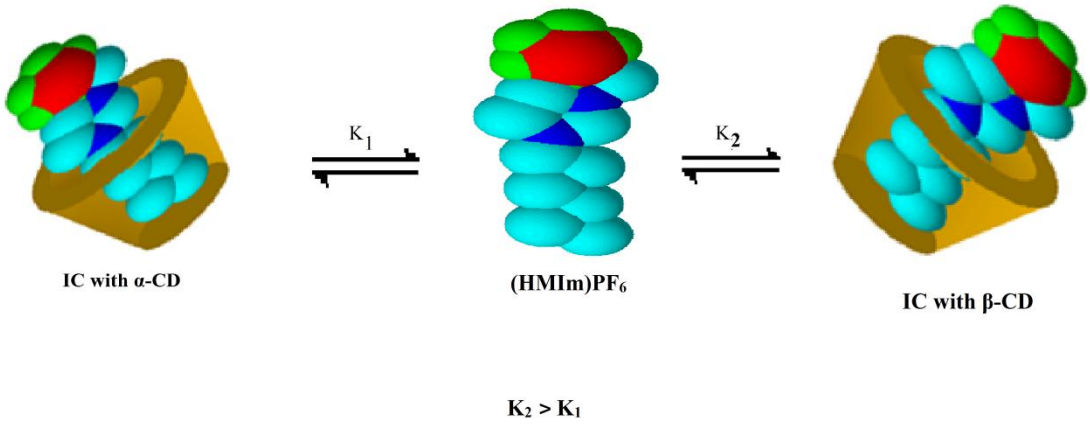

Scheme 3: Formation of inclusion complex with α-and β-CD

Scheme 3: Formation of inclusion complex

3.3. FT-IR spectroscopy

The FT-IR study is another trustworthy technique to probe the inclusion phenomena [29-31]. The FT-IR spectra of pure $(HMIm)PF_6$, cyclodextrins and their inclusion complexes are shown in **Fig.4.** Some characteristic frequencies of the ionic liquid are 2963 cm^{-1}, 3458 cm^{-1}, 1634.5 cm^{-1}, 1173 cm^{-1} and 1589 cm^{-1}probably for the groups of -C-H, =C-H, –C=N, -C-N and –C=C groups respectively and 3434.10 cm^{-1} and 3327 cm^{-1} for–OH group of α- and β-CD .(Fig.3).The frequencies for–O-H group of both the α- and β-CD shifted to the lower frequencies which may be considered due to the presence of hydrophilic-hydrophilic interaction between -OH groups of the CDs and the immidazolium part of ionic liquid. Thepeaks position for–C=N and –C-N groups

remained unchanged because these groups are situated outside the cavity of CD. The -C-H stretching frequency for alkyl group of ionic liquid is absent due to encapsulation of alkyl group into the cavity of CD.

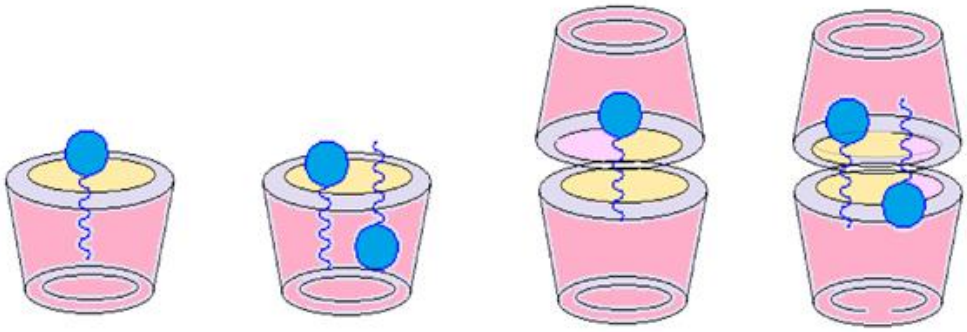

Scheme 4. Plausible host guest stoichiometry of inclusion complex**.**

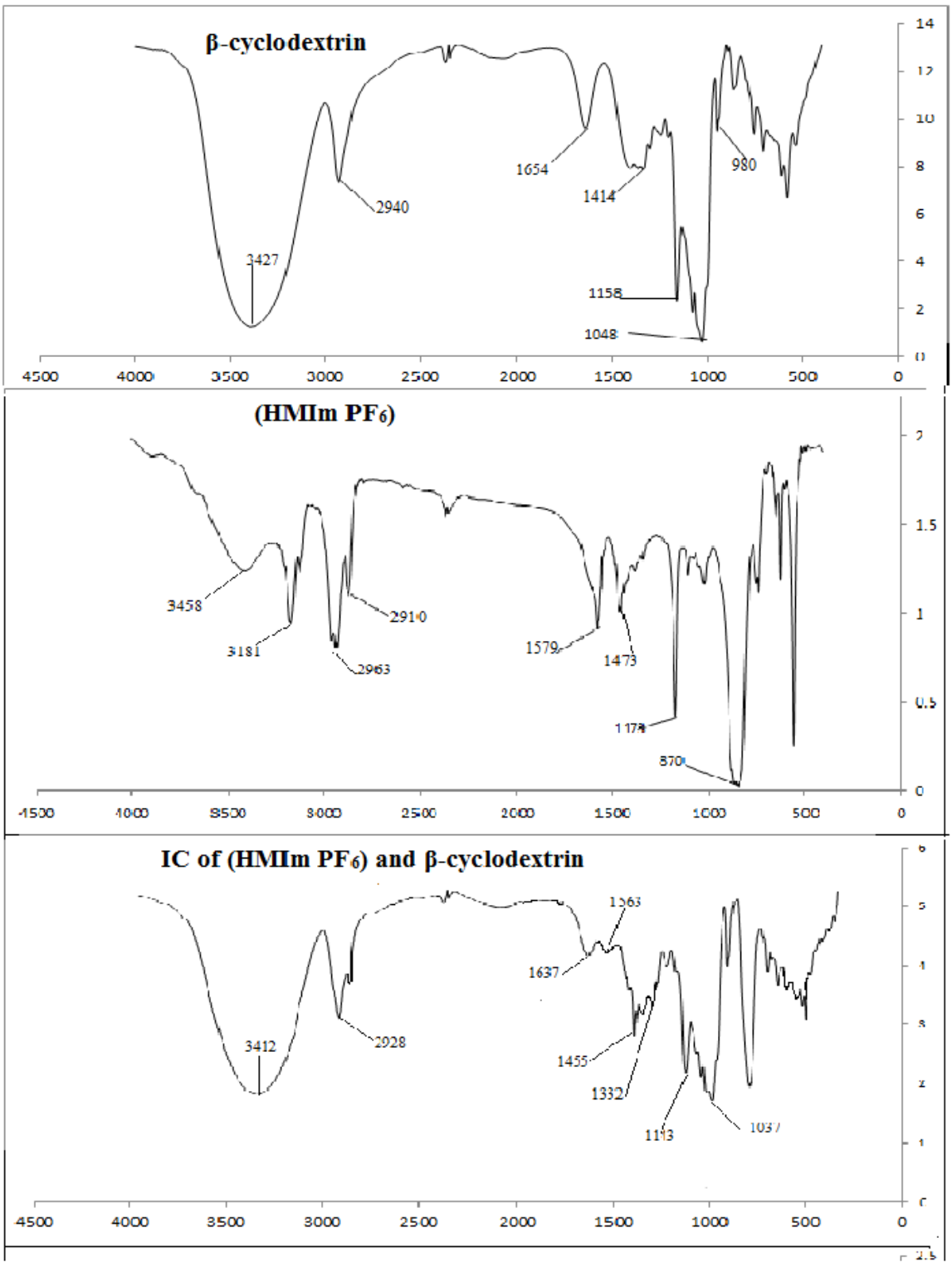
β-cyclodextrin
3427
2940
1654
1414
1158
1048
980
(HMIm PF6)
3458
3181
2963
2910
1579
1473
1178
870
IC of (HMIm PF6) and β-cyclodextrin
3412
2928
1637
1455
1332
1113
1363
4500
4000
3500
3000
2500
2000
1500
1000
500
0

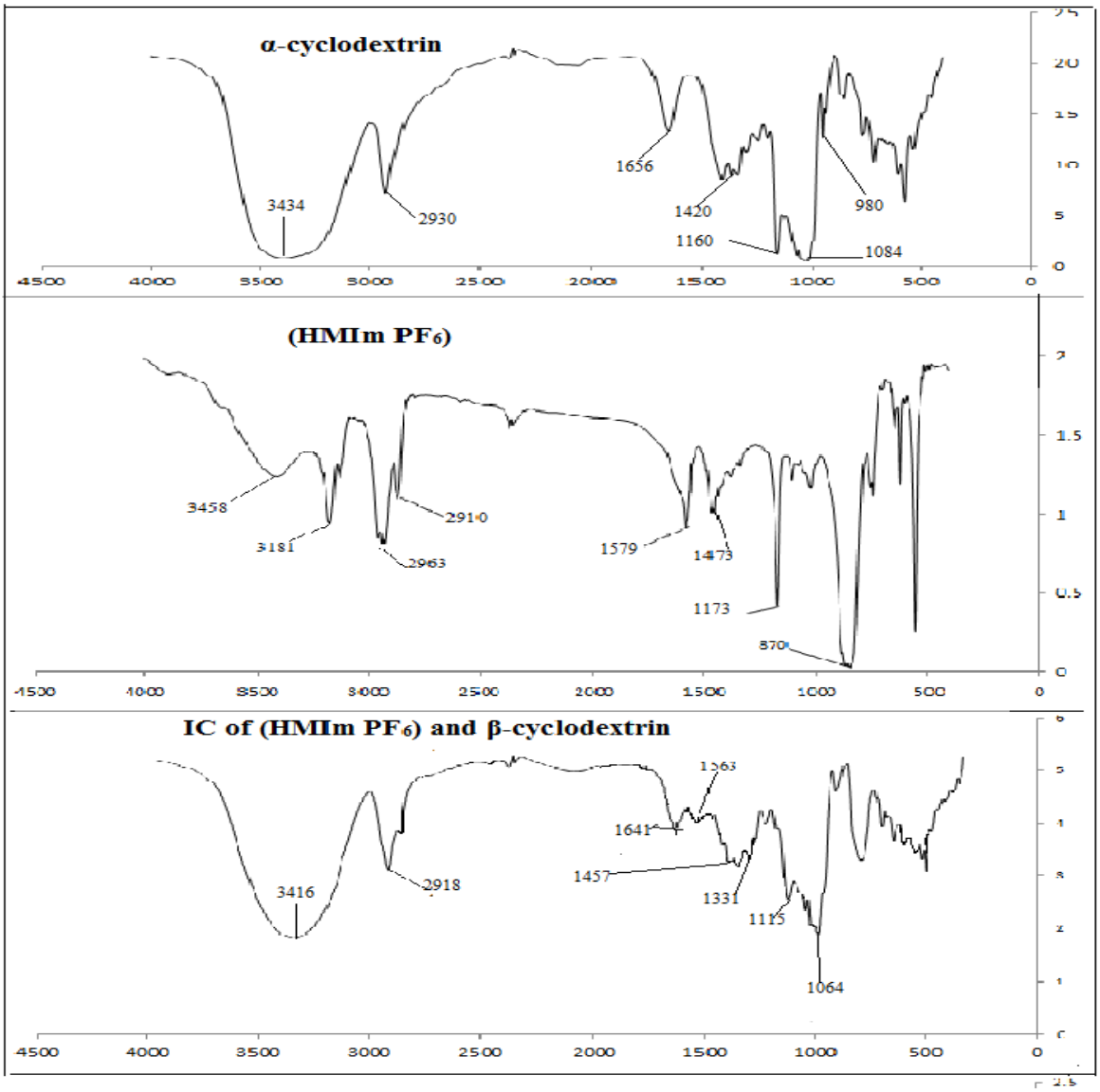

Fig.4. FTIR spectra of (HMIm)PF_6 and inclusion complexes of it in α-and β-CD at 298.15 K

The frequencies of different groups are as follows:
(HMIm)PF_6:3458 cm^{-1}(=C-H), 2963 cm^{-1}(-C-H), 1634 cm^{-1}(-C=N), 1589 cm^{-1}(C=C), 1473 cm^{-1}(Bending –CH2), 1406 cm^{-1}(Bending-CH2), 1173 cm^{-1}(-C-N)

α –Cyclodextrin:3434 cm^{-1}(Stetching of O-H), 2930 cm^{-1}(Stretching of –CH from –CH2), 1420 cm^{-1}(Bending –CH), 1160 cm^{-1}(Bending of C-O-C), 1080 cm^{-1}(stretching of C-C-O), 956 cm^{-1}(Vibration α-1,4 linkage)

β- Cyclodextrin:3327 cm^{-1}(Stetching of O-H), 2944 cm^{-1}(Stretching of –CH from –CH2), 1430 cm^{-1}(Bending –CH), 1158 cm^{-1}(Bending of C-O-C), 1030 cm^{-1}(stretching of C-C-O), 953 cm^{-1}(Vibration α-1,4 linkage)

(HMIm)PF_6/ α -CD inclusion complex:3316 cm^{-1}(Strtching of O-H of B-CD), 2918 cm^{-1}(Strtching of –C-H), 1457 cm^{-1}(Bending of –C-H), 1115 cm^{-1}(Bending of C-O-C), 1064 cm^{-1}(Stetching of C-C-O)

(HMIm)PF_6/ β -CD inclusion complex:3427 cm^{-1}(Strtching of O-H of B-CD), 2940 cm^{-1}(Strtching of –C-H), 1654 cm^{-1}(Stretching of –C=N), 1414 cm^{-1}(Bending of –C-H), 1158 cm^{-1}(Bending of C-O-C)

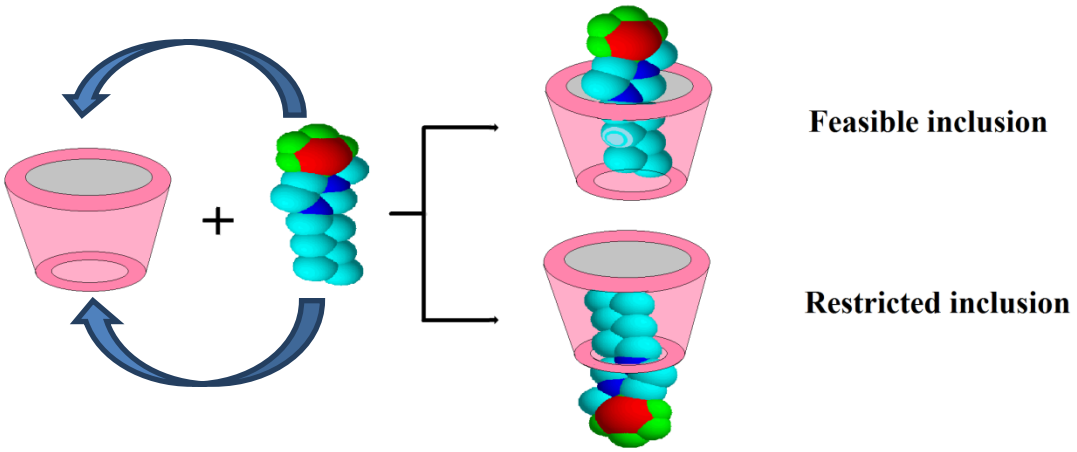

Scheme 5. Feasible and restricted inclusion complex formation of host-guest molecule

3.4. UV-Vis Spectroscopy Investigation

UV-Vis spectroscopy study also gives the clear indication of formation of host-guest inclusion complex [32]. In our present study we used methyl orange as a probe since the cyclodextrins and the $(HMIm)PF_6$do not absorb in the UV-Vis range.

Here the absorption spectra of methyl orange in presence of ionic liquid were measured at varying molarities of CDs**(Fig.5)**. It is found that absorbance increases increasing concentration of cyclodextrins when the concentration of the IL was kept unchanged.

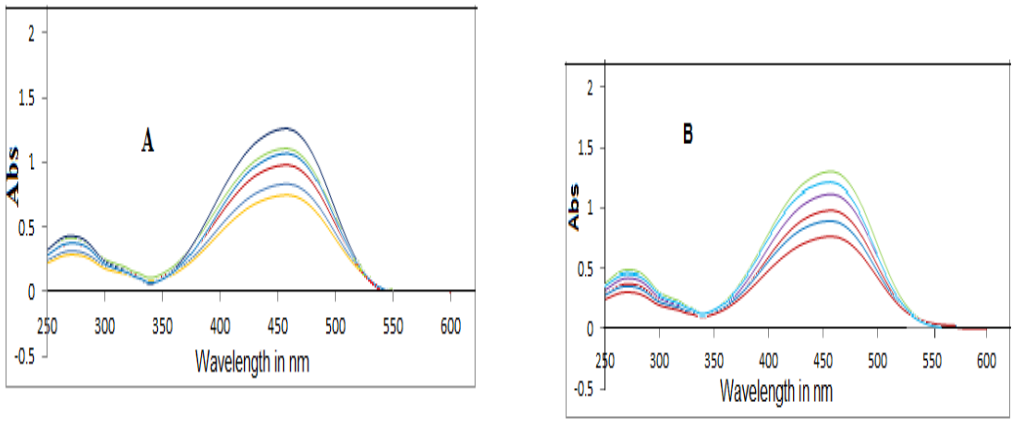

Fig.5. UV-vis spectra of methyl orange (MO) containing different concentration of (A) β-CD in $(HMIm)PF_6$ (B) α-CD in $(HMIm)PF_6$

The host-guest stoichiometry of inclusion complex may be evaluated by Job's plot calculated from UV-visible spectroscopy. The spectra were taken of ionic liquid and cyclodextrins mixture different concentration keeping the total concentration constant and shown in **Fig.6**.

Concentration ratio of ionic liquid, R = [IL]/([IL] + [CD])

The stoichiometry of host and guest of inclusion complex may be obtained by plotting the graph of ΔA×R vs. R [33-35].

Where, ΔA represents the absorbance of the studied IL without and with cyclodextrin at 298.15 K.

R = 0.5, 0.33 and 0.66 at the maxima of the graph signify the 1:1, 1:2 and 2:1 host-guest stoichiometry of the inclusion complexes. The R values in case of our studiedionic liquid, $(HMIm)PF_6$, is 0.5 which signify the 1:1 stoichiometry.

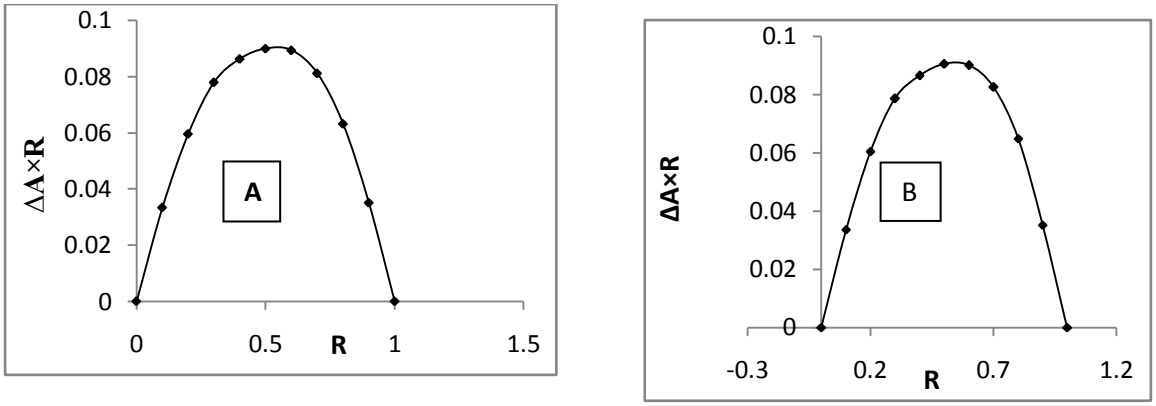

Fig.6. UV-vis spectra of methyl orange (MO) containing different concentration of (A) β-CD in $(HMIm)PF_6$ (B) α-CD in $(HMIm)PF_6$

The association constant of the inclusion complex for the cyclodextrin-ionic liquid system, $K_a$may be evaluated from the values of molar absorptivity of UV-Visible spectra. Here the spectra of the ionic liquid at constant molarity were taken with varying concentration of cyclodextrin in presence of the probe (methyl orange). We used the famous Benesi-Hildebrand equation to calculate the association constants (K_a) of I:I inclusion complex [36].

$$\frac{1}{\Delta A} = \frac{1}{\Delta\varepsilon K[Guest]} \times \frac{1}{[Host]} + \frac{1}{\Delta\varepsilon}$$

Where, ΔA denotes the absorbance difference of the ionic liquid in the presence and absence of CDs, Δε denotes the molar absorption co-efficient difference of IL in the presence and absence of CDs, [Guest] and [Host] represent the concentration of ionic liquid and cyclodextrin respectively.A plot of 1/ΔA versus 1/[CDs] (shown in **Fig.7)** gives a straight line with an intercept 1/Δε and a slope of $\frac{1}{\Delta\varepsilon K[Guest]}$. The association constant, K_a may be obtained by dividing the intercept with the slope of the double reciprocal plot at a certain concentration of ionic liquid. The K_a calculated from above equation for OMImBr/ α-CD system is $3.145 \times 10^3 M^{-1}$ and for OMImBr/ β-CD system is $3.192 \times 10^3 M^{-1}$.

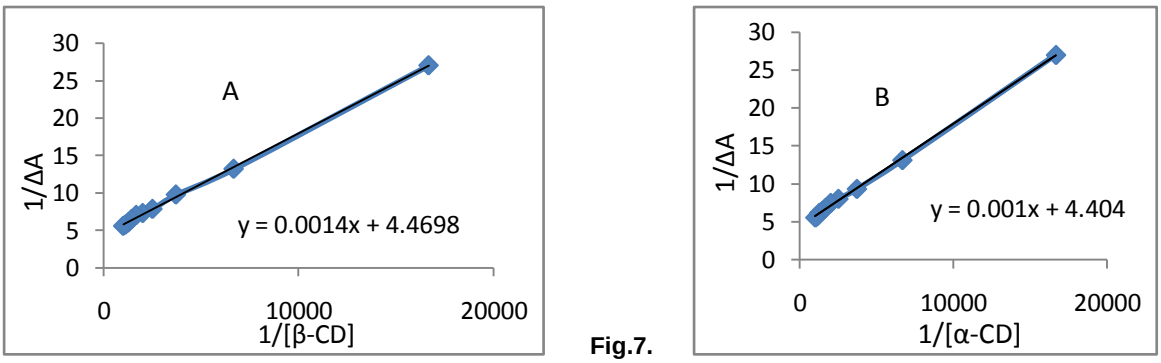

Fig.7. (A) Plot of 1/ΔA against 1/[β-CD]for examining stoichiometry of inclusion complexes .(B) Plot of 1/ΔA against 1/[α-CD] for examining stoichiometry of inclusion complexes.

3.5 ^{1}H NMR study

^{1}H NMR study also reveals the formation of host-guest inclusion complex of an ionic liquid into the cavity of cyclodextrins[37]. The ^{1}H NMR spectra of ionic liquid, cyclodextrins and their IC were carried out in D_2Oat 298 K and shown in **Fig.8**. Chemical shift of some protons of theinclusion complexes from CDs and IL may be regarded as the penetration of the alkyl part of IL inside the cavity of the CD molecule. We are aware that H3 and H5 protons of both cyclodextrins are situated inside the cavity whereas the H1, H2 and H4 protons are situated outside the cavity [38, 39]. In addition to that, H3 proton is located near the wider rim and H5 proton is situated near the narrower rim of the CDs. Due to the insertion of the alkyl part of the ionic liquid into the cavity of CDs, there was a significant up field chemical shift of the H3 and H5 protons of cyclodextrins and down field chemical shift of protons of alkyl part of the ionic liquid [40]. It is also seen that the chemical shift for H3 of IC is higher than

that of H5 protons which indicates that the hydrophobic alkyl part of IL enters into the hydrophobic cavity of CD through the wider rim of CD (**Scheme 5**). The significant chemical shift of the protons of N-methyl group may be regarded as presence of hydrophilic-hydrophilic interaction between the imidazolium part of the ionic liquid and the peripheral –OH group of nearby cyclodextrin molecules.

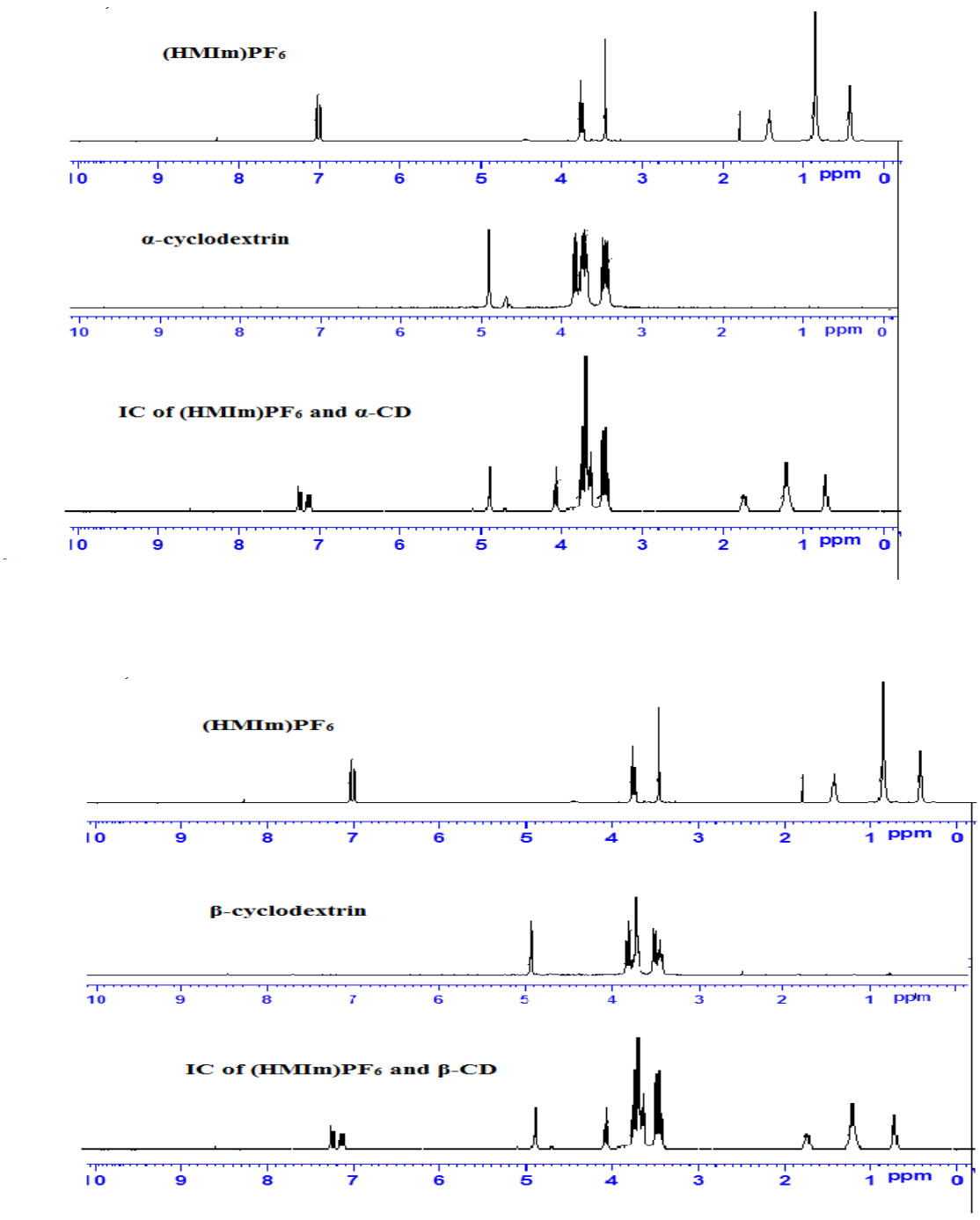

Fig.8. ^{1}H NMR spectra of $(HMIm)PF_6$ and inclusion complexes of it with α-and β-CD in D_2O at 299.15 K.

^{1}H NMR data:

(HMIm)PF6: [1H NMR (300 MHz, D2O)]: δ 0.409-0.443 (3H,m), 0.867(6H,m), 1.416-1.468 (2H, m), 1.803 (1H, S), 3.454 (3H, s), 3.733-3.774 (3H,m), 6.989-7.036 (1H,d)

α –Cyclodextrin:[^{1}H NMR (300 MHz, D_2O)]: δ 3.42-3.43 (6H, j=9.00Hz), 3.51-3.52 (6H, j=10Hz), 3.74-3.83 (18H, m), 3.87-3.91(6H, J=9Hz) 4.96-4.97 (6H, J=3Hz)

β –Cyclodextrin: [^{1}H NMR (300 MHz, D_2O)]: δ 3.41-3.42 (6H, j=9.00Hz), 3.53-3.56 (6H, j=10Hz), 3.75-3.77 (18H, m), 3.82-3.83(6H, J=9Hz) 4.97-4.98 (6H, J=3Hz)

(HMIm)PF6/ β –CD: [^{1}H NMR (300 MHz, D_2O)]: δ 0.72-0.754(3H,m), 1.209 (6H, s), 1.231-1.783 (2H, m), 3.425-3.498 (6H, m), 3.625-3.736(18H,m), 3.753-4.873(6H, m), 3.86-3.84(2H, s), 4.885 (2H, d), 7.245-7.256(1H,d),7.329-7.333(1H,d)

(HMIm)PF6/ α-CD: [^{1}H NMR (300 MHz, D_2O)]: δ 0.718-0.751(3H,m), 1.207 (6H, s), 1.228-1.779 (2H, m), 3.422-3.497 (6H, m), 3.622-3.733(18H,m), 3.757-4.874(6H, m), 3.81-3.80(2H, s), 4.883 (2H, d), 7.24-7.25(1H,d),7.324-7.328(1H,d)

3.6. 2D ROESY NMR

2D ROESY NMR study is a sophisticate technique to probe the formation of inclusion complexes [41, 42]. We know that two neighboring protons situated within a distance of 0.4 nm can exert a nuclear overhauser eff ect which may be ascertained by 2D ROESY NMR (rotating-frame NOE spectroscopy). The ROESY NMR spectra of inclusion complexes of (HMIm)PF_6withboth the cyclodextrins are displayed in **Fig.9**. The H3 and H5 protons of CDs which are located inside the cavity exert nuclear overhauser eff ect with the protons attached with the alkyl part of IL. As a result cross-peakscorresponding to the H3 and H5 protons are found in the ROESY NMR spectra inclusion complexes of (HMIm)PF_6 and cyclodextrins.

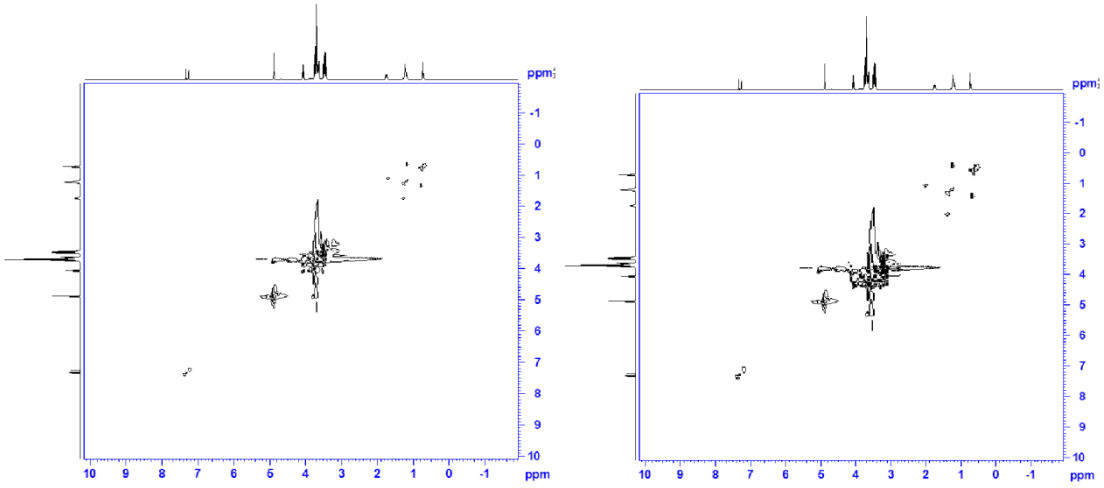

Fig.9. NMR ROSEY spectra of inclusion complexes of (A) (HMIm)PF_6 and α-CD (B) (HMIm)PF_6 and β-CD

IV. Conclusion

The size of the non-polar part of the guest molecule and the diameter of the cavity of cyclodextrins are the main determining factor of the formation of inclusion complex. The diameters of cavity of α- and β-CD are 4.7–5.3 Å and 6.0–6.5 Å respectively. We also discussed earlier that the both cyclodextrins have hydrophobic inside and hydrophilic outside. This kind of special characteristic provides a suitable environment for the non-polar part of guest ionic liquid to be encapsulated inside the cavity of cyclodextrin. The alkyl part of an ionic liquid is held inside the cavity of CD through hydrophobic- hydrophobic interaction without forming or breaking any bond. The imidazolium part of ionic liquid is located outside the wider rim of CD and form H-bonds with the –OH groups present at the periphery of another CD molecule. Overall studies reveal that the complexation between (HMIm)$PF_6$and cyclodextrins is of 1:1 stoichiometry and(HMIm)PF_6fits better in the cavity of β –CD than α-CD.

V. Acknowledgement

We convey our heartfelt gratitude to UGC, New Delhi, India (No. 540/27/DRS/2007, SAP-DSR) and UGC-RGNF India (No.F117.1/201617/RGNF201517SCWES1846 and F.1/2012-13/RGNF- 2012-13-SC-WES-17229) for funding the project. Prof. M.N. Roy is indebted to the UGC, New Delhi, India for giving him one-time

Grant-in-Aid [No.F4-10/2010 (BSR)] todevelop research facilities for the scholars. We express our gratefulness to the SAIF, North Eastern Hill University, Shillong, India for performing the NMR analysis.

References

[1.] E. Leyva, E. Moctezuma, J. Strouse, M. A. Garcla-Garibay, Journal of Inclusion Phenomena and Macrocyclic Chemistry. 39 (2001) 41-46.

[2.] Y. Kawaguchi, T. Nishiyama, M. Okada, M. Kamachi, A. Harada, Complex Formation of poly (ε-caprolactone) with cyclodextrins, Macromolecules, 33 (2000) 4472-4477.

[3.] M.E. Brewster, T. Loftsson, Cyclodextrins as pharmaceutical solubilizers, Adv Drug Deliv Rev. 59 (2007) 645-666.

[4.] A. Harada, T. Nishiyama, Y. Kawaguchi, M. Okada, M. Kamachi, Preparation and Characterization of Inclusion Complexes of Aliphatic Polyesters with Cyclodextrins, Macromolecules, 30 (1997) 7115-7118.

[5.] S. S. Satav, R. N. Karmalkar, M. G. Kulkarni, N. Mulpuri and G. N. Sastry, Formation of linear polymers with pendant vinyl groups via inclusion complex mediated polymerization of divinyl monomers, J. Am. Chem. Soc. 128 (2006) 7752-7753.

[6.] S. H. Cho, S. Y. Kim, S. I. Lee, Y. M. Lee, Hydroxypropyl-3-cyclodextrin inclusion complexes for transdermal delivery: preparation, inclusion properties, stability and release behaviour, J. Ind. Eng. Chem. 12 (2006) 50-59.

[7.] X. Zhu, J. Sun, J. Wu, Spectrofluorimetric determination of trace Co(II) in aqueous samples with quinalizarin-β-cyclodextrin inclusion complex, Talanta. 72 (2007) 237–242.

[8.] H. Jiao, S. Goh, S. Valiyaveettil, Inclusion Complexes of Poly(4-vinylpyridine)−Dodecylbenezenesulfonic Acid Complex and Cyclodextrins, Macromolecules 35 (2002) 3997-4002

[9.] N.L. Strutt, R.S. Forgan, J.M. Spruell, Y.Y. Botros, J.F. Stoddart, , Monofunctionalized pillar [5] arene as a host for alkanediamines, J. Am. Chem. Soc.133 (2011) 5668-5671.

[10.] X. Chi, M. Xue, Y. Yao, F. Huang, Redox-responsive complexation between a pillar [5] arene with mono (ethylene oxide) substituents and paraquat, Org. Lett, 15 (2013) 4722-4725.

[11.] T.F. A. Azemi, M. Vinodh, F.H. Alipour, and A.A. Mohamod, Constitutional Isomers of Pentahydroxy-Functionalized Pillar[5]arenes: Synthesis, Characterization, and Crystal Structures, J. of Org. Chem., 82 (20), (2017) 10945-10952

[12.] X. Chi, M. Xue, Y. Yao, F. Huang, Formation of a Cyclic Dimer Containing Two Mirror Image Monomers in the Solid State Controlled by van der Waals Forces, Org. Lett. 15 (2013) 4722-4725.

[13.] T. Welton, Room-Temperature Ionic Liquids. Solvents for Synthesis and Catalysis, Chem. Rev. 99 (1999) 2071-2083.

[14.] K. Huang, X. Zhang, D.W. Armstrong, Ionic cyclodextrins in ionic liquid matrices as chiral stationary phases for gas chromatography,J. Chromatogr. A 1217 (2010) 5261-5273.

[15.] K. A. Connors, The stability of cyclodextrin complexes in solution, chem. Rev. 97(1997) 1325–1357.

[16.] R. Gopal , M.A. Siddique, A study of ion-solvent interactions of some tetra alkyl- ammonium and common ions in N-methyl acetamide from apparent molar volume data, J. of Phy. Chem. 72 (1969) 1814–1817.

[17.] H.M. Zerth, N.M. Leonard, R.S. Mohan, Synthesis of Homoallyl Ethers via Allylation of Acetals in Ionic Liquids Catalyzed by TrimethylsilylTrifluoromethanesulfonate, Org. Lett. 5 (2003) 55–57.

[18.] M. N. Roy, D. Ekka, S. Saha and M. C. Roy, Host–guest inclusion complexes of α and β-cyclodextrins with α-amino acids, RSC Adv. 4 (2014) 42383–42390.

[19.] A. Pineiro, X. Banquy, S. Perez-Casas, E. Tovar, A. Garcia, A. Villa, A. Amigo, A. E. Mark and M. Costas, On the Characterization of Host-Guest Complexes: Surface Tension, Calorimetry, and Molecular Dynamics of Cyclodextrins with a Non-ionic Surfactant, J. Phys. Chem. B. 111 (2007) 4383–4392.

[20.] S.D. Qi, S.Y. Cui, X.G. Chen, Z.D. Hu, Rapid and sensitive determin- ation of anthraquinones in Chinese herb using 1-butyl-3- methylimidazolium-based ionic liquid with beta-cyclodextrin as modifier in capillary zone electrophoresis, J. Chromatogr. A. 1059 (2004) 191–198.

[21.] R. Lu, J. Hao, H. Wang, and L. Tong, Determination of Association Constants for Cyclodextrin–Surfactant Inclusion Complexes: A Numerical Method Based on Surface Tension Measurements, J. of Col. and Int. S. 192 (1997) 37–42.

[22.] Y.A. Gao, Z.H. Li, J.M. Du, G.Y. Zhang, Preparation and Characterization of Inclusion Complexes of β-Cyclodextrin with Ionic Liquid, Chem. Eur. J. 11 (2005) 5875-5880.

[23.] R.Palepu, J.E. Richardson, V.C. Reinsborough, Binding constants of. beta. -Cyclodextrin/Surfactant Inclusion by Conductivity Measurements, Langmuir. 5 (1989) 218-221

[24.] A. Apelblat, E. Manzurola and Z. Orekhova, Electrical Conductance Studies in Aqueous Solutions with Glutamic Ions, J. Solution Chem. 36 (2007) 891–900.
[25.] G. Law, P.R. Watson, Surface Tension Measurements of N-Alkylimidazolium Ionic Liquids, Langmuir. 17 (2001) 6138–6141.
[26.] D. Evans, S. Wellington, J. Nadis, E. Cussler, The conductance of cyclic polyether-cation complexes, J. Solut. Chem.1 (1972) 499-506.
[27.] G. Khayatian, S. Shariati, M. Shamsipur, Conductance study of the thermodynamics of binding of some macrocyclicpolyethers with Tlþ ion in dimethylformamide-acetonitrile mixtures, J. Inclusion Phenom. Macrocycl. Chem. 45 (2003) 117-121.
[28.] S. Barman, M.N. Roy, Hollow circular compound-based inclusion complexes of an ionic liquid, RSC Adv. 6 (2016) 76381-76389.
[29.] S. Saha, A. Roy, M.N. Roy, Mechanistic investigation of inclusion complexes of a sulfa drug with a- and b-cyclodextrins, Ind. Eng. Chem. Res. 56 (2017) 11672–11683
[30.] W. Zhang, X. Gong, Y. Cai, C. Zhang, X. Yu, J. Fan and G. Diao, Investigation of water-soluble inclusion complex of hypericin with β-cyclodextrin polymer, Carbohydr. Polym. 95 (2013) 366–370.
[31.] S. Milovanovic, D. Markovic, K. Aksentijevic, D. B. Stojanovic, J. Ivanovic, I. Zizovic, Application of cellulose acetate for controlled release of thymol, Carbohydr. Polym, 147 (2016) 344–353.
[32.] J. S. Negi, S. Singh, Spectroscopic investigation on the inclusion complex formation between amisulpride and γ-cyclodextrin, Carbohydr. Polym. 92 (2013) 1835–1843.
[33.] Y. Sueishi, T. Ide, Inclusion complexation of methyl orange with β-cyclodextrin in a roomtemperature ionic liquid, Z. Phys. Chem., 218 (2004) 829-835.
[34.] P. Job, Formation and stability of inorganic complexes in solution, Annali di ChimicaApplicata 9 (1928) 113–203.
[35.] J.S. Renny, L.L. Tomasevich, E.H. Tallmadge, D. B. Collum, Angew, Method of continuous variations: applications of job plots to the study of molecular associations in organometallic chemistry, Chem. Int. Ed. 52 (2013) 11998–12013.
[36.] Caso, L. Russo, M. Palmieri, G. Malgieri, S. Galdiero, A. falanga, C. Isernia, R. Iacovino, Investigating the inclusion properties of aromatic amino acids complexing beta-cyclodextrins in model peptides, Amino Acids 47 (2015) 2215–2227.
[37.] H.A. Benesi, J.H. Hildebrand, A Spectrophotometric Investigation of the Interaction of Iodine with Aromatic Hydrocarbons, J. Am. Chem. Soc. 71 (1949) 2703-2707.
[38.] J. V. Caso, L. Russo, M. Palmieri, G. Malgieri, S. Galdiero, A. Falanga, C. Isernia and R. Iacovino, Investigating the inclusion properties of aromatic amino acids complexing beta-cyclodextrins in model peptides, Amino Acids. 47 (2015) 2215–2227
[39.] V. Sindelar, M. A. Cejas, F. M. Raymo, W. Chen, S. E. Parker and A. E. Kaifer, Supramolecular assembly of 2,7-dimethyldiazapyrenium and cucurbit[8]uril: A new fluorescent host for detection of catechol and dopamine, Chem. Eur. J. 11 (2005) 7054–7059.
[40.] T. Wang, M. D. Wang, C. Ding and J. Fu, Mono-benzimidazole functionalized β-cyclodextrins as supramolecularnanovalves for pH-triggered release of p-coumaric acid, Chem. Commun. 50 (2014) 12469–12472.
[41.] J. V. Caso, L. Russo, M. Palmieri, G. Malgieri, S. Galdiero, A. Falanga, C. Isernia, R. Iacovino, Investigating the Inclusion Properties of Aromatic Amino Acids Complexing beta-Cyclodextrins in Model Peptides, Amino Acids 47 (2015) 2215-2227.
[42.] E. Bednarek, W. Bocian, J. Pozna´nski, J. Sitkowski, N. S. Sosnowska and L. Kozerski, Complexation of steroid hormones: prednisolone, ethinyloestradiol and estriol with ß- cyclodextrin. An aqueous 1 H NMR study, J. Chem. Soc. Perkin Trans. 2, (2002) 999–1004.
[43.] T. Stalin, K. Srinivasan, K. Sivakumar and S. Radhakrishnan, Preparation and characterizations of solid/aqueous phases inclusion complex of 2,4-dinitroaniline with β-cyclodextrin, Carbohydr. Polym., 107 (2014) 72–84.

International Journal of Innovation Engineering and Science Research

Open Access

Analysis of Rural Road Networks Considering Redundancy

Jagat Kumar Shrestha
Civil Engineering Department, Pulchowk Campus,Institute of Engineering, TU Kathmandu, Nepal

ABSTRACT

A new evaluation method for the redundancy of rural road-links is introduced in this paper. The study provided the distance based link redundancy measures. The methodological contribution in this paper comes in exploiting the evaluation concept with a view of Link Redundancy Index (LRI). This method will be useful to the decision makers as a simple tool for predicting and monitoring the road performance to improve the rural road network to a robust network for the mobility of goods and services in rural hilly areas.

Keywords—rural road network, redundancy, Link Redundancy Index

I. INTRODUCTION

Rural road networks are the backbone of physical and social development in hilly areas of Nepal. The networks are being developed in Nepal but in a haphazard way. This has created many landslides making the hill environment very vulnerable to disasters. On the other hand, we need sufficient level of connectivity in the network even in a reserve level to serve in the situation of blockage and disaster. These networks are to be developed optimally considering the need of the road in the hilly regions of Nepal and cost of construction and maintenance. There is always a trade-off between them to utilize scarce resources in an optimal way. Hence, ananalysis of rural road networks considering redundancy has been envisioned in this research which will develop a scientific tool and helpful to make rational decisions in construction, maintenance and development of rural road networks in Nepal to save huge junk of resources.

In 2014, Arniko highway in Nepal was suffered from floods. It was the international highway to China, only the gateway to trade to China. There was no alternative link to the Chinese boarder. Further, the road was heavily damaged by the 2015 Gorkha Earthquake. Still the road is in the blockage stage. Also, despite major calamities, blockage of mountainous road due to landslides is the common problem during every monsoon in Nepal. Further in rural areas, the problem is more common as the hill roads are commonly earthen and gravel roads. The earthen roads are pliable in the dry seasons only. Due to this reason, most of the people residing the mountainous hilly region has no options for alternative connection by roads in the time of natural disaster and accidents. The problem of delivering goods and services to the affected people and the region is the common problem and a critical issue. Hence, alternative links to the existing road network is required to minimize the degree of the problem. However, cost is always associated with any intervention. Hence, the investment is to be based on the need and identification of the situation and the predicting the possible intervention based on a rational decision making tool.This work is devoted to develop the tool that evaluates the existing situation and propose the optimal intervention which will be useful to the decision makers to plan and develop an optimal road network considering the spare links for route diversity.

II. REDUNDANCY IN ROAD NETWORKS

The concept of redundancy has been studied in different disciplines including reliability engineering, water distribution system, internet network, and so on. In reliability engineering, redundancy is the existence of more than one means for accomplishing a given function, and each means of accomplishing the function is not necessarily identical [10]. Redundancy in water distribution system is defined as the existence of alternative pathways from the source to demand nodes or excess capacity in normal operating conditions when some components of the system become unavailable [11]. In transportation network, Redundancy is one of the four “Rs” (Robustness, Redundancy, Resourcefulness, and Rapidity) proposed byBruneau et al. (2003) [9] for assessing resiliency of the system. Some researchers have introduced variousmeasures for assessing the resiliency of transportation networks and redundancy is one of those measures. Forexample,

Godschalk (2003) [11] and Murray-Tuite (2006) [12] defined redundancy as the number of functionally similarcomponents which can serve the same purpose, and hence the system does not fail when one component fails. Arelevant concept of redundancy is diversity, which refers to a number of functionally different components thatprotect the system against various threats (e.g., alternative transport modes). Similarly, Goodchild et al. (2009)[8] defined redundancy as theavailability of multiple alternate routing options in the freight transportation network. Jenelius (2010) [2] proposed the concept of redundancy importance to consider the importance of links as backup alternatives whenother links in the network are disrupted. Two measures (i.e., flow-based and impact-based) were proposed toquantify the redundancy importance. The flow-based measure considers a net traffic flow that is redirected to thebackup links and the impact-based measure considers an increased travel time (cost) due to the rerouting effect.However, these two measures assess only the localized redundancy importance of a transportation network. In otherwords, they are not able to capture the diversity of alternatives, an important property for measuring networkredundancy. He argued that the diversity of available routes when the primary choice is inoperative needs to beexplicitly considered in the redundancy characterization. Furthermore, the route diversity alone may not be a sufficientmeasure of redundancy as it lacks the interaction between transport demand and supply (i.e., congestion effect dueto limited network capacity). Indeed, redundancy should also indicate the state of backup or spare capacity of anetwork. However, in the case of rural road network, the capacity of a network is not a problem.Therefore, the concept of redundancy can be limited and dealt with single dimension of route diversity.

III. EVALUATION OF REDUNDANCY IN ROAD NETWORKS

Some researchers has evaluated redundancy considering the static conditions of the network such as **road density** in the road transport network. Jenelius (2009) [1]stated that a higher road density to some extent guarantees a higher availability of alternative paths. However, road density only considers the fully operational link status e.g. by adding the link length to the whole network length or subtracting link length when the link is fully closed. Hyder Consulting (2010) [3] estimated the redundancy value of a link as the total number of motorways,A roads, and B roads within a 10 kilometre radius of the link (A roads – 'major roads intended to provide large-scale transport links within or between areas; Broads – roads intended to connect different areas, and to feed traffic between A roads and smaller roads on the network' [4]. However, that will not be the situation in rural areas like in mountainous terrain in Nepal. Both approaches [4] [2] introduced static, purely topological indicators. Graph theory has also been used to quantify the redundancy of networks by using a number of indices, such as a clustering coefficient and the number of independentroutes [5]. The clustering coefficient, also known as transitivity, is a measure of redundancy as it represents the overall probability for the network to have interconnected adjacent nodes [6], which could be measured by different indicators [5]. The clustering coefficient is a significant characteristic of road transport network redundancy, though, it only considers the directly neighbouring nodes or links and neglects possible capacity limitations which may restrict redundancy.

Jenelius (2010) [2] introduced a 'redundancy importance' concept as a new way to study the role of the link in network redundancy. The author quantified the importance of redundancy in two ways. Firstly, the importance of flow-based redundancy was calculated as the weighted sum of the difference in flow arising from the closure of all links in the network. Secondly, an impact based redundancy importance measure was computed as the weighted sum of the difference in the impact measure arising from the closure of all links in the network.

Average path length concept is also used in network topology that is defined as the average number of steps along the shortest paths for all possible pairs of network nodes. It is a measure of the efficiency of information or mass transport on a network.

Average path length is one of the three most robust measures of network topology, along with its clustering coefficient and its degree distribution. The average path length distinguishes an easily negotiable network from one, which is complicated and inefficient, with a shorter average path length being more desirable.

IV. AVERAGE PATH LENGTH

In complex networks, the distance d_{ij} between nodes i and j is defined as the minimumnumber of the sides connecting the two nodes; the network diameter is defined as the largestdistance of two random nodes; the average value of the distances of all the node pairs of thecomplex networks is marked with L, which reflects the degree of separation between nodesand can be calculated by the following formula[7]:

$$L = \frac{1}{N(N-1)} \sum_{i \neq j} d_{ij} \quad (1)$$

where N is the node number.
The path length of urban road network is the distance from one intersection to anotherand the average path length L refers to the average value of the shortest path length betweenall intersection pairs.

V. DEFINITION OF THE LINK REDUNDANCY INDEX (LRI)

The earliest studies on road network disruption provided the concept of road network vulnerability [13], and such provisionwas the starting point of the increase in the number of studies on road network performancein terms of vulnerability or robustness. The studies on vulnerability orrobustness of road network are often associated with link criticality analysis, which is usedfor ranking the importance of road network component like bridges [13]. As a network component is more critical, the malfunctionof the component would give more severe damage to the network system, and the vulnerabilityof certain area including the component would then be greater. Thus, analysingcriticality of each component under disruptive situation would be the pre-process of vulnerabilityanalysis. Note that the term in this paper, criticality, has a similar meaning to theterm, 'importance' used by Jenelius, Petersen, andMattsson (2006) and Jansuwan and Chen(2015), which represents only the degree of consequence of disruptive event regardless ofthe probability of such event occurring.

Several measures of road link criticality have been proposed, and the measures providedby Jenelius, Petersen, and Mattsson (2006) [14] are the prime examples. The importance measure proposed by Jenelius, Petersen andMattsson (2006) [14] depends on the increase of travel cost for all OD pairs of the non-failedlinks within a network. They derived the values of importance measure for eachroad link in the form of increased travel time per vehicle. Scott et al. (2006) [15] proposed ameasure called Network Robustness Index (NRI), which is an expression of increased travelcost when a link is failed.

In the similar fashion, in the context of rural hill road network where the network is uncapacited as the traffic volume is very less (less than 100 vehicles/day), we can define a new measure, the Link Redundancy Index (LRI), for evaluating the critical importance of agiven roadlink (i.e., network link) to the overallsystem as the change in travel-time cost associated withrerouting all traffic in the system.For this situation In formulating the measure, let the distance d_{ij} between nodes i and j is defined as the shortest distance between the node i and node j. The link-specific index isderived in two steps.

First, the system-wide, we can calculate average path length removing the link, La, is given by the followingequation:

$$La = \frac{1}{N(N-1)} \sum_{i \neq j} d_{ij}\, \delta_{ij} \quad (2)$$

Where,

$$\delta_{ij} = \begin{cases} 1; if\ link\ a\ is\ not\ removed \\ 0; \text{otherwise} \end{cases}$$

Second, this La is compared to the system-wide, L incurred when all links are present in the network(i.e., the base case) which canbe calculated using Eq. (1).

$$R = La - L \quad (3)$$

R is the value of the LRI for link a in units such as km. Although we define Eq. (3) in terms of changein distance, the index can be generalized tomeasure change in monetary cost.

VI. CASE STUDY IN THE REAL ROAD NETWORK

The case study is carried out to demonstrate the concept of LRI in a rural road networks.For this purpose, the road network (171 km) of BhimsenGaupalika of Gorkha district, Nepal has been considered whichcovering101.25 km2. A Gaunpalika is the second lowest administrative division of Nepal. For the test instance, the Minimum Spanning Tree (MST) of the road network is formed to identify the backbone links in the network. In the hilly road networks, the MST is taken as the minimum level of connectivity necessary for the region to provide access to the settlements and public facilities. Furthermore, additional links are

necessary in the network for the diversity for the time of disruption of any link. This network contains 93 nodes and 106 links. The network contains all type of links including tracks of the under construction roads.

Figure 1: BhimsenGaupalika road network

Table1: LRI in BhimsenGaupalika road network

S.N.	Removed Link ID	Length (km)	Average Length (km)	R=La-L
1	Not Removed	171.401	11.324	
2	117	167.342	11.726	0.40
3	145	170.553	12.332	1.01
4	146	169.774	12.580	1.26
5	157	170.291	13.042	1.72
6	160	168.847	12.143	0.82
7	216	167.628	11.781	0.46
8	220	169.928	12.086	0.76
9	209	169.664	12.330	1.01
10	206	170.228	12.215	0.89
11	113	170.427	11.731	0.41
12	114	170.724	11.589	0.26
13	111	167.198	11.319	(0.01)
14	194	170.341	11.935	0.61

Based on the analysis, Table 1 has been obtained in which link 157 in the road network (Figure 1) has the highest LRI and is the most critical link in the network. There must be the spare links for route diversity to divert the traffic through the link. Hence, a circuit of network is required, the role of non-backbone links (black thick links in Figure 1) which are in circuit with the link 157 are now important to quickly bypass the traffic. Otherwise, the traffic should detour a long distance to reach the nearby nodes, and will have huge impact on cost and importance of delivery of goods and services during emergency. In this context, constituting appropriate management strategies for road links in a certain network system is an important process for minimizingperformance loss of the system under disaster situations. This information is also important for maintenance andrepair works period. For this matter, evaluatingthe LRIindex of each link in road network has to be performed,because such information would be useful while constituting the development strategiesfor road links in the network.

VII. CONCLUSION

A new evaluation method for the redundancy of rural roadlinks is introduced in this study. The study provided the distance based link redundancy measures.Such measure is derived by comparing the behaviours of the road network in normal and eventsituations.

The methodological contribution in this paper comes in exploiting the evaluation conceptwith a view of Link Redundancy Index (LRI). As a link of a network isdisrupted, the path for some vehicles would be altered and this would cause a local influenceof traffic. Due to the local influence, traffic in the disrupted network should detour a long distance in the network, and so will impact the cost and performance of the network. Such phenomenondue to the local influence can be captured for evaluating the LRIof the disrupted link.

An advantage of using this LRI measure is that we may not even require afull microscopic simulation to predict the network performance loss. Particularly in termsof monitoring the performance in real-time, the information of OD demand distribution ordriver's routing is very difficult to be obtained in real-time a cost endeavour. So, instead of usingODtravel information, with the LRI measure,the road performance loss also can be predicted only with the simple link length data collection in the rural road network. This method will be useful to the decision makers as a simple tool for predicting and monitoring the road performanceto improve the rural road network to a robust network for the mobility of goods and services in ruralhilly areas.

REFERENCES

[1] E.Jenelius, Network structure and travel patterns: explaining the geographical disparities of road network vulnerability. Journal of Transport Geography, 17, 2009, pp.234-244.

[2] E.Jenelius,Redundancy importance: Links as rerouting alternatives during road network disruptions. In: Procedia Engineering 3: 1st Conference on Evacuation Modeling and Management, 2010, pp.129–137.

[3] Hyder, Network Resilience and Adaptation: Phase 1 Final Report, 2010 Highway Agency, UK.

[4] DfT, Department for Transport, Winter Resilience in Transport: an assessment of the case for additional investment, 2011. [Accessed 10-05-2014]. Available from: https://www.gov.uk/government/uploads/system/uploads/attachment_data/file/4557/an-assessment-of-the-case-for-additional-investment.pdf

[5] S.Boccaletti, V.Latora, Y.Moreno, M.Chavez and D.U. Hwang, Complex networks: Structure and dynamics. Physics Reports, 424, 2006 pp.175-308.

[6] J. P.Rodrigue, C.Comtois and B.Slack, The geography of transport systems, Routledge, 2009.

[7] D. J. Watts and S. H. Strogatz, Collective dynamics of 'small-world' networks. Nature, 6684(393), 1998, 440–442.

[8] A. Goodchild,E.Jessup, E.McCormack, D.Andreoli, S.Rose, C.Ta, K. Pitera, Development and Analysis ofa GIS-based Statewide FreightData Flow Network, 2009.

[9] M.Bruneau, S. E. Chang, R. T. Eguchi, G.C. Lee, T.D. O'Rourke, A.M.Reinhorn, M.Shinozuka, K.Tierney, W.Wallace, D.von Winterfelt, A Framework to Quantitatively Assess and Enhance the Seismic Resilience of Communities, EERI Spectra Journal, Vol.19, No.4, 2003 pp.733-752.

[10] P.D.T.O'Connor,Practical reliability engineering, fourth edition. 2010, John Wiley & Sons, LTD.

[11] D.Godschalk, Urban Hazard Mitigation: Creating Resilient Cities. Natural Hazards Review 4(3): 2003, 136-4 143.

[12] P.Murray-Tuite, A Comparison of Transportation Network Resilience under Simulated System, 2006.

[13] K.Berdica, L.G. Mattsson, Vulnerability: a model-based case study of the road network in Stockholm. Critical Infrastructure, 2007, 81-106.

[14] E.Jenelius, T.Petersen, L.G. Mattsson, Importance and exposure in road network vulnerability analysis. Transportation Research Part A 40 (7), 2006, 537-560.

[15] D. M.Scott, D. C. Novak, L.Aultman-Hall, andF.Guo, Network robustness index: a new method for identifying critical links and evaluating the performance of transportation networks. Journal of Transport Geography, 2006, 14(3), 215-227.

International Journal of Innovation Engineering and Science Research

Open Access

Computer and laboratory research of condition of MIM 4140 alloy after injection molding and sintering

Denis Chemezov[1], Dmitry Kononov[2], Anatoly Molkov[3], Lyudmila Smirnova[4], Elena Bogomolova[5]
[1, 3, 4, 5]Vladimir Industrial College, Russian Federation
[2]Vladimir State University Named After Alexander and Nikolay Stoletovs, Russian Federation

ABSTRACT

The results of a computer simulation of an injection molding process in a mold (changing of liquid phase of melt during filling and crystallization) and laboratory research of condition of MIM 4140 alloy after heat treatment are presented in the article. Color contours showing a value of linear shrinkage and porosity of a casting material before heat treatment are obtained. It is determined that maximum linear shrinkage and porosity occur in an area of the casting bottom. A general picture of condition of inner layers of the castings material before and after heat treatment is given.

Keywords *– a casting, linear shrinkage, porosity, filling, crystallization, sintering.*

I. INTRODUCTION

MIM technology is processes of injection molding and sintering of castings which are made of special alloys [1 – 8].

Comparison of linear shrinkage of the casting material “Plunger” before and after heat treatment was performed in the article [9]. Linear shrinkage of the casting material after sintering is 17 – 19% from the casting dimensions to sintering in accordance with requirements specification for development of design documentation and manufacturing of a mold. Increasing of pore dimensions in surface layers of material was determined after heat treatment of the casting.

The required accuracy of dimensions and shape, surfaces roughness and material structure of the casting after injection molding and sintering are achieved by careful manufacturing of the mold, compliance of casting modes and proportions selection of the chemical elements of alloy. Analysis of this technological process before operation of the mold in production conditions is recommended to perform in special computer programs. Changing of liquid phase of melt during cooling, linear shrinkage, porosity and other casting defects of the casting material after crystallization (a semi-finished product before heat treatment) are determined in special modules of these programs. Comparison of the simulation results and laboratory researches will allow to make a conclusion about the accuracy of a performed computer calculation.

II. MATERIAL AND METHOD

The simulation of the injection molding process of the castings was performed in the computer program LVMFlow. The solid model of the casting “Plunger” is presented in the Fig. 1.

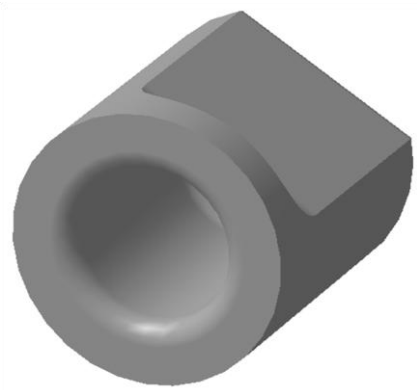

Fig. 1. The model of the casting "Plunger".

The created casting model had the following dimensions and elements: a maximum outer diameter – 7.01 mm, a total length – 8.14 mm, the hole diameter – 3.9 mm, the hole depth – 6.43 mm, radii on an outer and inner side of bottom – 0.35 mm. The casting was made of MIM 4140 alloy. A weight of one casting is 1.1 g.

Conditions of the computer simulation of injection molding (filling of a chamber of a molding machine by melt, injection phase of melt into the mold and melt cooling) are presented in the summary table 1.

TABLE I. DESCRIPTOR INFORMATION.

Mesh						
	Box dimension		***Casting position***			***Number of cells***
along X, mm	81.250		40.494			65
along Y, mm	201.250		100.321			161
along Z, mm	60.000		30.000			48
Size of cells, mm	1.25					
Total cells	502320					
Casting cells	60052					
Boundary conditions						
	Low					***High***
YZ plane	Normal conditions					Normal conditions
XZ plane	Normal conditions					Normal conditions
XY plane	Normal conditions					Normal conditions
Materials temperature						
Materials	***T, °C***					
MIM 4140	180.000					
1044	20.000					
Air	20.000					
Air gap (interfacial heat transfer model)						
	Coefficient, %					
v Upper	100.00					
v Lateral	100.00					
v Lower	100.00					
Mold parameters						
Mold material	***Total emissivity***		***Gas-permeability, 10^{-6} m^2/Pa×s***			***Radiolucency***
1044	0.93		1.53			-
Air	-		-			1.00
Shrinkage calculation model						
Medium gravity influence						
Influence coefficient			50			
"Feeding" pressure, Bar			0.000			
Alloy	***Compr., 1/Mbar***	***CLF up, %***	***CLF down, %***	***CLFpres, %***	***CLF Niyama, %***	***Property created***
MIM 4140	30.00	70.00	30.00	24.00	3.00	by phases
Quasi-equilibrium model calculation, without segregation						
With taking gas into account at filling						
Initial gas pressure in mold, Bar			1.000			
Gas pressure outside mold, Bar			1.000			
With convection						
Aggressive AMG						
The Gauss-Seidel method						

Gatings				
X, mm	***Y, mm***	***Z, mm***	***Boundary conditions***	
40.45	183.12	43.76	Heat radiation	20.00
Pouring type				
Lip pouring				
Friction factor	***Pressure height, mm***	***Teta***		***Fi***
1.000	80.000	20.000		0.000
Stream diameter, mm	***Flow, kg/s***	***Stream area, mm^2***		
8.000	0.408	50.265		

High casting properties of melt and excess pressure allow to perform the filling process of the mold in full volume. Coefficient of turbulence of melt when filling of the mold was taken 0.3.

The model of a gating system and the model of the chamber of the molding machine for injection molding of eight castings are presented in the Fig. 2.

The chamber model of the molding machine ARBURG Allrounder 270C 400-100 was built to the right of the gating system model of the mold. Melt enters into a feeder and then into the gating system of the mold from the chamber of the molding machine. Eight castings are poured at the same time into the mold. The feeder diameter is the hole diameter of a heat treated steel sprue bushing (the length of 50.5 mm). Through hole in the bushing is performed conical. The maximum hole diameter of the sprue bushing is 3 mm, the minimum hole diameter of the sprue bushing is 2 mm. The central hole in the castings is formed by eight rods placed in the mold cavity. The chamber length of the molding machine was 173.501 mm, which corresponds to capacity of 102461.4 mm^3. Effective mass of a piston at specified dimensions of the chamber of the molding machine was 0.048 kg.

The chamber model of the molding machine was filled by melt in the volume of 4.531% (or 0.032 kg). Movement phase of the piston in the chamber of the molding machine occurs after filling of the required volume of melt (no downtime after filling). Pressure on the piston was set by the value of 1667.139 Bar in accordance with requirements specification for development of design documentation and manufacturing of the mold. Maximum allowable pressure on the piston is 2000 Bar.

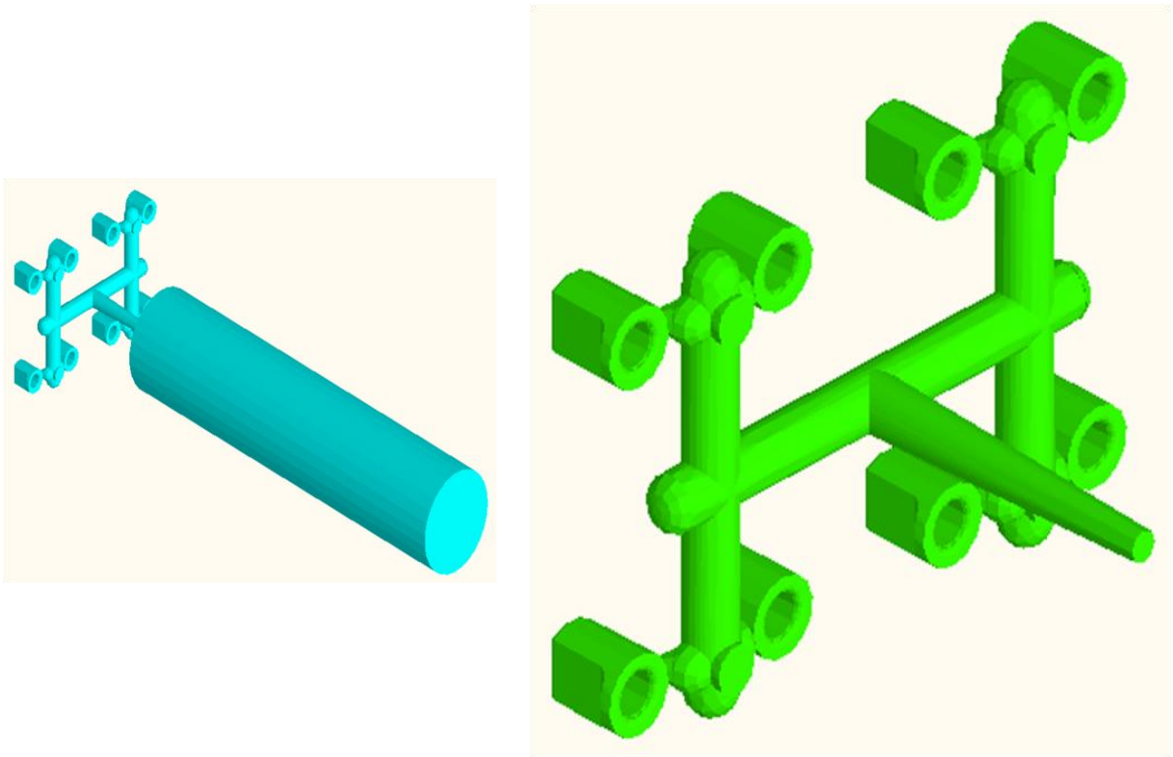

Fig. 2. The model of the gating system of the multicavity mold for injection molding.

The computer calculation was completed when complete filling of the mold cavity by melt (100%) and cooling melt in the mold to a temperature below the solidus temperature.

III. Result and discussion

Steps sequence of the mold filling by melt is presented in the Fig. 3.
The following stages show on the figure:
A and B – filling of the chamber model of the molding machine by melt;
C – F – movement of the piston in the chamber model of the molding machine;
G – O – injection phase of melt into the forming cavity of the mold.
The piston model was not displayed at the calculation. The diameter of a pressing part of the piston was equal to the diameter of the chamber model of the molding machine. So as the presented process lasts less than one second then crystals nucleation is not observed and liquid phase in melt is not less than 95%. Filling time of the mold by melt was 0.095 s.
Steps sequence of melt crystallization (cooling) in the mold is presented in the Fig. 4.
First of all, the castings are subjected to crystallization (cooling), so as their volume is less than the volume of the gating system of the mold. The significant volume of material remains in the gating system of the mold after crystallization, which is an irrational using of material for this casting process.
Time crystallization of melt in the mold was 0.678 s.
Total time of injection molding was 0.773 s.

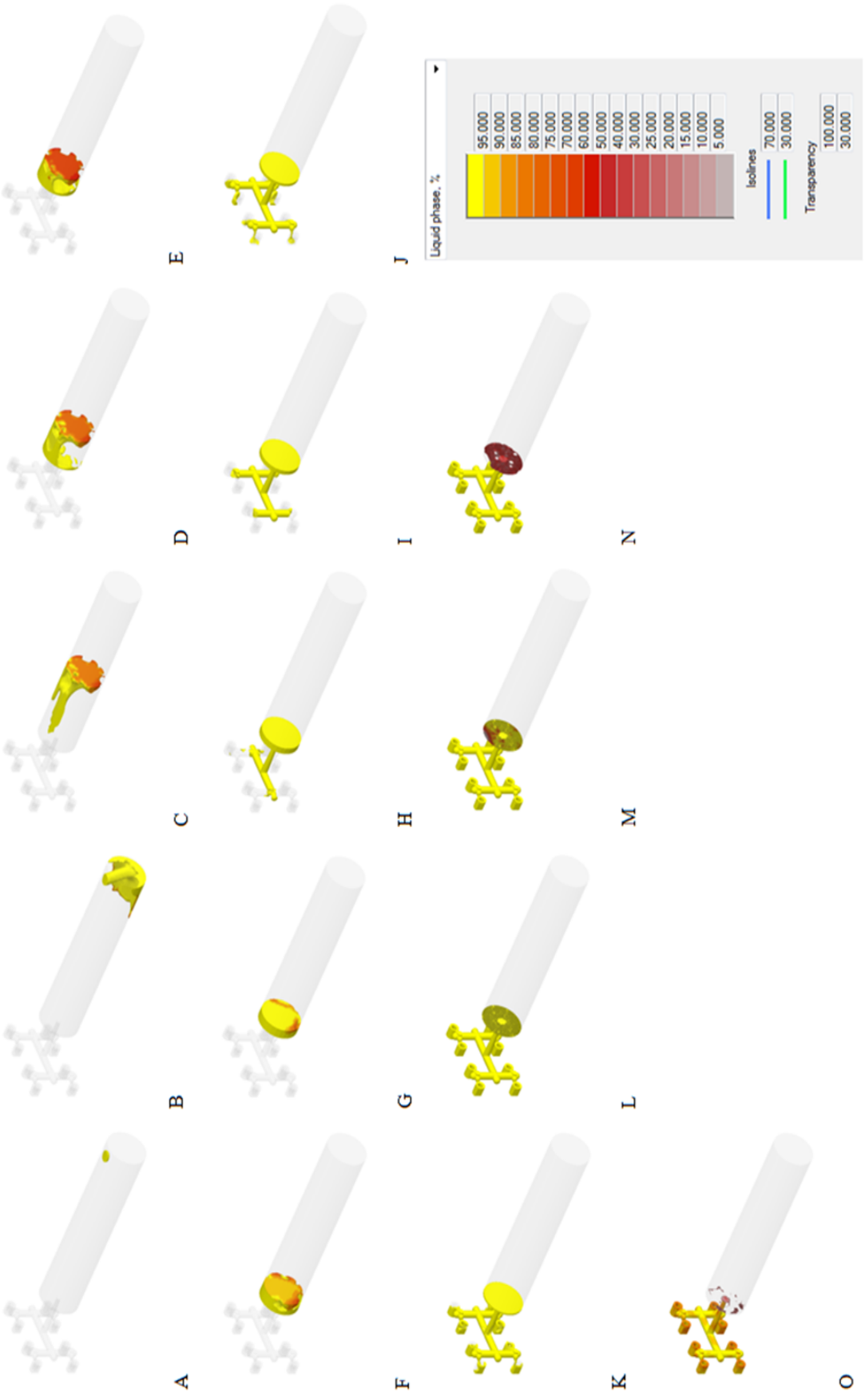

Fig. 3. Sequence of the mold filling by melt.

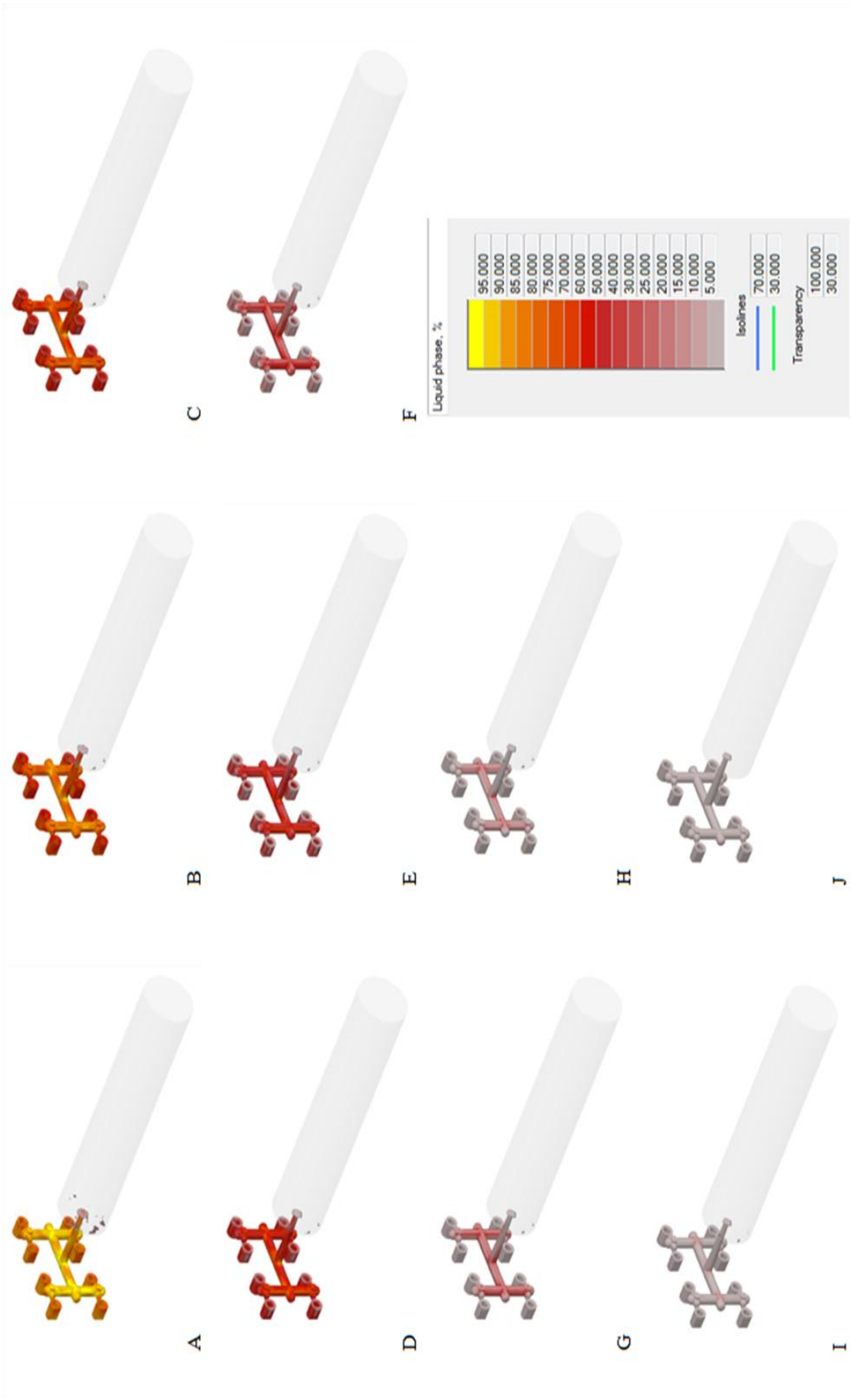

Fig. 4. Sequence of melt crystallization in the mold.

Linear shrinkage of the casting material after crystallization in the mold is presented in the Fig. 5. The color contours on the casting models show linear shrinkage of material in percentage. Maximum linear shrinkage of the casting material after crystallization is observed in the upper part of the mold. Linear shrinkage of material on side walls of the castings was determined in the range of 1 – 10%. The casting bottom is subjected to linear shrinkage in the range of 10 – 20%.

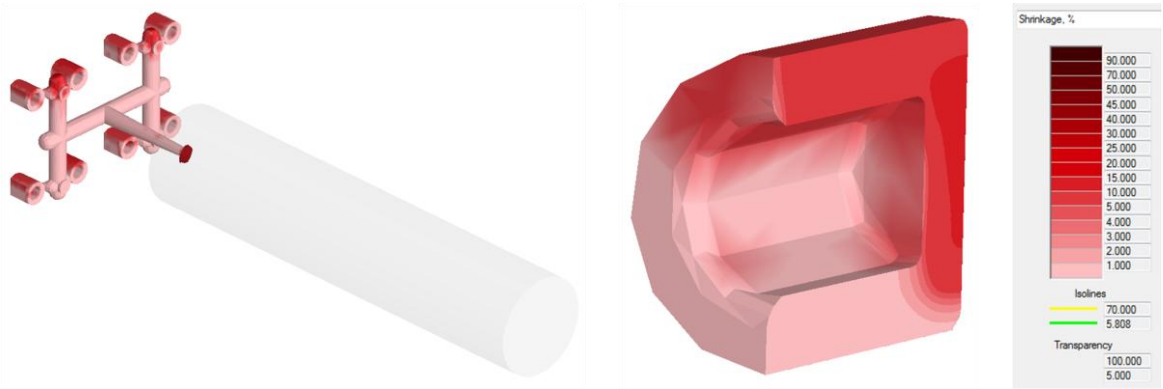

Fig. 5. Linear shrinkage of the casting material after crystallization.

Porosity of the casting material after crystallization in the mold is presented in the Fig. 6. Probability of porosity formation in the casting material after crystallization is predicted by the Niyama criterion. The Niyama criterion is found as the ratio of temperature gradient to cooling rate of the casting material at the end of time interval of crystallization. The less the Niyama criterion, the more probability of porosity formation in the casting material. Porosity is formed on the outer diametrical surface and in the area of bottom of the castings in accordance with the color contours.

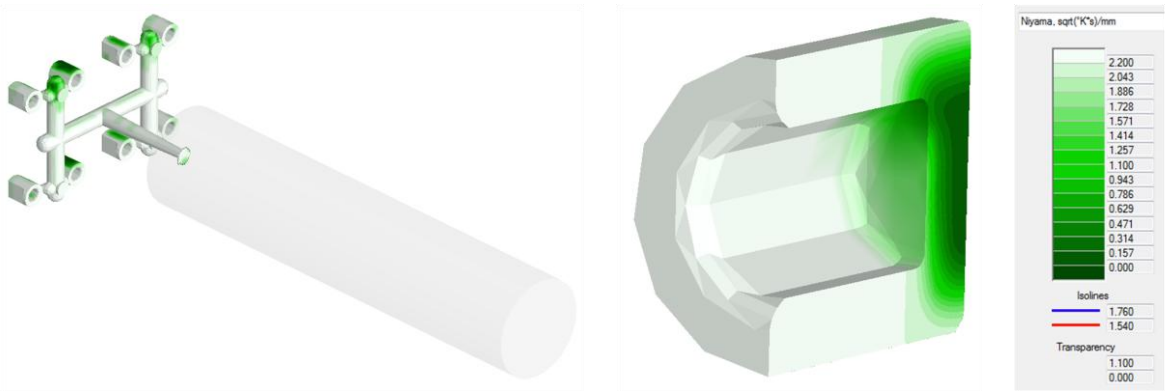

Fig. 6. Porosity of the casting material after crystallization.

Condition of the casting material after injection molding in the mold and before heat treatment is presented in the Fig. 7.

Fig. 7. Condition of the casting material after injection molding.

Longitudinal cutting of the casting into two parts after injection molding was performed by a knife, so as material was fragile and not subjected to electrical discharge machining. Material structure on the cut surface of the casting is homogeneous. Small pores are clearly visible on the casting surface. Prediction of porosity formation in the casting material corresponds to the color contours of porosity on the casting model by 85%.

Condition of the casting material after injection molding and heat treatment is presented in the Fig. 8.

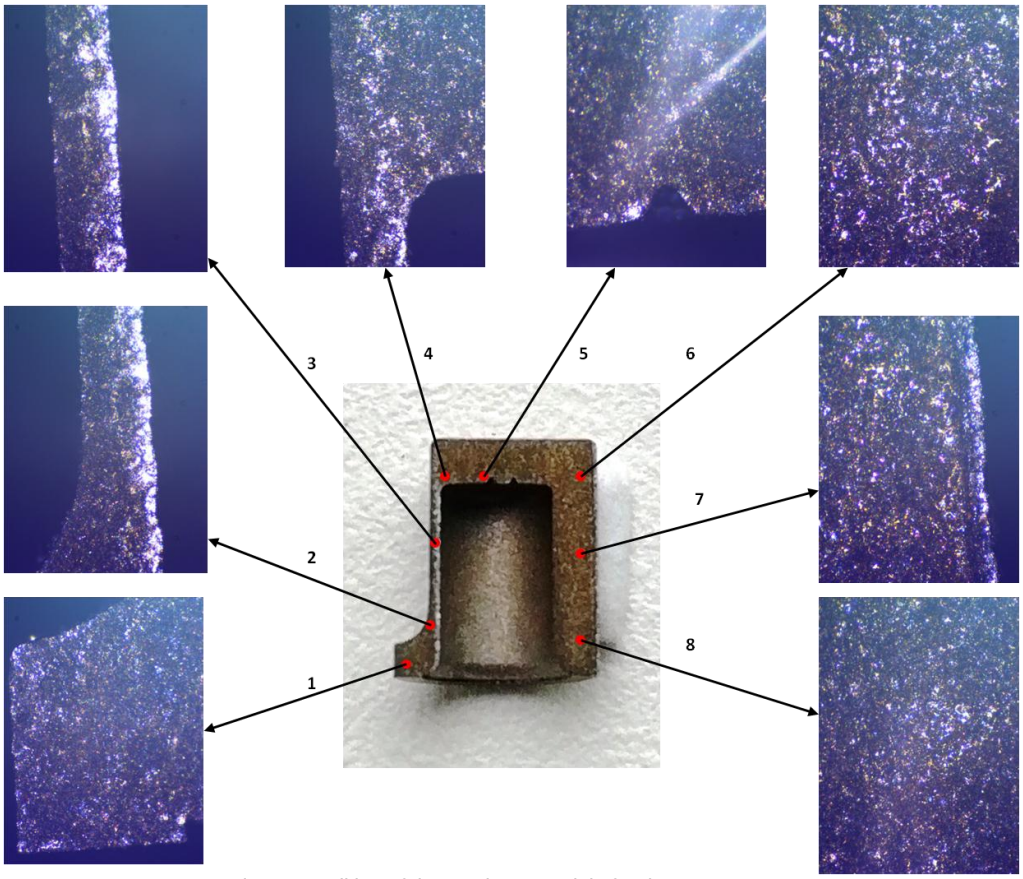

Fig. 8. Condition of the casting material after heat treatment.

Longitudinal cutting of the casting into two parts after heat treatment was performed on the electrical discharge machine. Photos of condition of the casting material were obtained by means of objective lens of the model Olympus Mplan 5 with a digital camera. The photos show that structure of the casting material remains homogeneous, and pores increased in dimensions. Thus, thermal influence leads to removing of binder material and hardening of the casting. White shine on the surface has remained from a copper wire when cutting of the casting on the electrical discharge machine.

IV. Conclusion

Based on the results of the computer simulation of the injection molding process of MIM 4140 alloy and laboratory research of condition of the casting material after sintering, the following conclusions can be made:

1. Crystallization time of the castings in the mold is calculated and the ratio of liquid phase in melt is determined during injection molding of MIM 4140 alloy.
2. Linear shrinkage and porosity of the real casting after injection molding correspond to the calculated values of linear shrinkage and porosity of the casting model by 85%. This says about the high accuracy of the computer simulation of the injection molding process. The Niyama criterion is determined for casting of MIM 4140 alloy (from 0 to 2.2 $\frac{\sqrt{^{\circ}K \times s}}{mm}$).

3. Binder material is removed after heat treatment. Structure density of the casting material does not change before and after heat treatment. Pores dimensions in the casting material after sintering are changed.

REFERENCES

[1] Romashov N.A., Karapuzov O.G. A new method for improving the quality of "Green" details. Journal "Politechnical student journal" of BMSTU, №2, 2016. Pp. 1 – 8. (in Russ.).

[2] Pogodina E. Powder injection molding. Plastics, no. 6, 2013. Pp. 34–36 (in Russ.).

[3] Semenov A.B., Gavrilenko A.E., Semenov B.I. Powder synthesis technology for complicated shaped parts made of superalloys: AM and/or PIM (foreign and local experience). 2d int. conf. "Additive technologies: present and future". Moscow, FGUP VIAM Publ., 2016. 784 p. (in Russ.).

[4] Baril E., Thomas Y., Hetu J.-F., Pelletier S. Powder injection molding (PIM) for low cost manufacturing of intricate parts to net-shape. URL: http://www.dtic.mil/dtic/tr/fulltext/u2/a524692.pdf (accessed 25.06.2018).

[5] Heaney D. Handbook of metal injection molding. Woodhead Publishing Ltd, 2012. 586 p.

[6] Injection Moulding MIM parts. URL: http://www.cnder.com/Upload/PicFiles/2009.1.12_16.28.4_4954.jpg (accessed 25.06.2018).

[7] Application for MIM. URL: http://www.design-chnology.org/injectionmoulding2.htm (accessed 25.06.2018).

[8] Metal Injection Molding. URL: http://www.custompartnet.com/wu/metal-injection-molding (accessed 25.06.2018).

[9] Chemezov D. Properties of MIM 4140 Alloy After Injection Molding and Sintering. International Journal of Innovation Engineering and Science Research, Volume 2, Issue 1, 2018. Pp. 10 – 14.

International Journal of Innovation Engineering and Science Research

Open Access

The scaling invariant spaces for fractional Navier-Stokes equations

Xiaona Cui
College of Mathematics and Information Science
Henan Normal University
China

ABSTRACT

In this paper, we consider the scaling invariant spaces for fractional Navier-Stokes in the Lebesgue spaces $L^p(R^n)$ and homogeneous Besov spaces $\dot{B}^s_{p,q}(R^n)$ respectively.

Keywords—*scaling invariant spaces; fractional Navier-Stokes; parameters; Besov spaces*

I. INTRODUCTION

In this note, we study the scaling invariant spaces of the fractional Navier-Stokes equations (also called generalized Navier-Stokes equations) on the half-sapce $R^{1+n}_+ = (0,\infty)\times R^n, n \geq 2$:

$$\begin{cases} u_t + (-\Delta)^\beta u + (u\cdot\nabla)u - \nabla\pi = 0, R^{1+n}_+, \\ \nabla\cdot u = 0, R^{1+n}_+, \\ u(x,0) = u_0, R^{1+n}_+, \end{cases} \qquad (1)$$

where $\beta \in (\frac{1}{2}, 1)$. The fractional Navier-Stokes equations (1) has been studied by many authors. Lions [1] obtain the global existence of the classical solutions when $\beta \geq \frac{5}{4}$ in the 3D case. Wu [2] got the n dimension result for $\beta \geq \frac{1}{2} + \frac{n}{4}$, in [3] considered the existence of solution in $\dot{B}^{1+\frac{n}{p}-2\beta}_{p,q}(R^n)$. There are many other results in [4-8] and the reference there.

In this paper, we mainly study the road of finding the scaling invariant spaces for fractional Navier-Stokes equations in Lebesgue space $L^p(R^n)$ and the homogeneous Besov space $\dot{B}^s_{p,q}(R^n)$, where the space $L^p(R^n)$ is the set of function f satisfying

$$\|f\|_{L^p(R^n)} = \left(\int_{R^n} |f(x)|^p \, dx\right)^{\frac{1}{p}} < \infty, 0 < p < \infty,$$

and the homogeneous Besov space is the subset of the dual of the Schwartz space $S'(R^n)$, with the boundedness of the semi norm

$$\|f\|_{\dot{B}^s_{p,q}(R^n)} = \left(\sum_{j\in Z} 2^{qjs} \|\dot{\Delta}_j f\|^q_p\right)^{\frac{1}{q}} < \infty.$$

II. RESULTS AND PROOFS

Before we give our main theorem, we firstly give a lemma which will be used later.

Lemma 2.1 (The scaling invariant spaces) The scaling invariant spaces satisfy

$$u_\lambda(t,x)=\lambda^{2\beta-1}u(\lambda^{2\beta}t,\lambda x)\ ,\ \pi_\lambda(t,x)=\lambda^{4\beta-2}u(\lambda^{2\beta}t,\lambda x),(u_0)_\lambda(x)=\lambda^{2\beta-1}u_0(\lambda x).$$

Proof: We firstly proof the scaling transforms of the functions $u(t,x)$, $\pi(t,x)$, $u_0(x)$ are

$$u_\lambda(t,x)=\lambda^a u(\lambda^b t,\lambda^c x)\ ,\ \pi_\lambda(t,x)=\lambda^d\pi(\lambda^e t,\lambda^f x),(u_0)_\lambda(x)=\lambda^g u_0(\lambda^h x)$$

where a,b,c,d,e,f,g,h are non-negative integers to be determined later. If (u,π,u_0) are the solution of the system (1), then we take $(u_\lambda,\pi_\lambda,(u_0)_\lambda)$ into the system (1) and find the relationships between a,b,c,d,e,f,g,h such that $(u_\lambda,\pi_\lambda,(u_0)_\lambda)$ are also the solution of the system (1).

We calculate that

$$(u_\lambda)_t=\lambda^{a+b}u_t(\lambda^b t,\lambda^c x)\ ,$$
$$(-\Delta)^\beta u_\lambda=\lambda^a\cdot\lambda^{2\beta c}(-\Delta)^\beta u,$$
$$\nabla\cdot u_\lambda=\lambda^{a+b}\nabla\cdot u(\lambda^b t,\lambda^c x),$$
$$\nabla\pi_\lambda=\lambda^{d+f}\nabla\pi(\lambda^e t,\lambda^f x).$$

Putting all the equations above into the first equation of the system (1), we have

$$\lambda^{a+b}u_t(\lambda^b t,\lambda^c x)+\lambda^{a+2\beta c}(-\Delta)^\beta u+\lambda^a\cdot\lambda^{a+c}u(\lambda^b t,\lambda^c x)\cdot\nabla u(\lambda^b t,\lambda^c x)-\lambda^{d+f}\nabla\pi(\lambda^e t,\lambda^f x)=0,$$

For the aim that $(u_\lambda,\pi_\lambda,(u_0)_\lambda)$ are also the solution of the first equation of the system (1), we need that

$$a+b=a+2\beta c=2a+c=d+f\ .$$

We note that the above equations have 3 equations with 6 unknown variables, there are infinity solutions with 3 free variables. And through computing, we have

$$a+b=a+2\beta c\ \Rightarrow b=2\beta c,$$
$$a+b=2a+c\ \Rightarrow b=a+c,$$

here we can choose $c=1$, thus $b=2\beta$ and $a=2\beta-1$. After that we take $f=1$, due to $a+b=d+f$, that is $2\beta-1+2\beta=d+1$, we have $d=4\beta-2$. The variable e can be arbitrary.

Since the term π can be expressed by u , we know that the important work of the determination of the scaling invariant spaces is to choose the parameters in $u_\lambda(t,x)$, that is the determination of the parameters a,b,c,d,e,f,g,h. The method is by the fact that if the function $u(t,x)$ satisfies the system (1), so does $u_\lambda(t,x)$, thus we determine the parameters in the scaling invariant spaces.

Next, we obtain the scaling invariant spaces X for the system (1), that is we find the spaces X , such that $\|u\|_X=\|u_\lambda\|_X$, where $u_\lambda(x)=\lambda^{2\beta-1}u(\lambda x)$. We consider the cases that X is the Lebesgue space $L^p(R^n)$ and the homogeneous Besov space $\dot{B}^s_{p,q}(R^n)$ respectively. The first result is that X is of the Lebesgue space $L^p(R^n)$.

Theorem 2.1 Fractional Navier Stokes equations (1) are scaling invariant on $L^p(R^n)$, if and only if $p=\dfrac{n}{2\beta-1}$.

Proof: It is sufficient to show that $\|u\|_{L^p(R^n)}=\|u_\lambda\|_{L^p(R^n)}$. Due to $u_\lambda(x)=\lambda^{2\beta-1}u(\lambda x)$, we have

$$\|u_\lambda\|_{L^p(R^n)}=\left(\int_{R^n}|\lambda^{2\beta-1}u(\lambda x)|^p\,dx\right)^{\frac{1}{p}}.$$

Set $\lambda x = x'$, thus $x = \frac{x'}{\lambda}$, $dx = \frac{1}{\lambda^n} dx'$, we get

$$\|u_\lambda\|_{L^p(R^n)} = \left(\int_{R^n} |\lambda^{2\beta-1} u(x')|^p \frac{1}{\lambda^n} dx' \right)^{\frac{1}{p}}$$
$$= \lambda^{2\beta-1-\frac{n}{p}} \left(\int_{R^n} |u(x')|^p \, dx' \right)^{\frac{1}{p}} = \lambda^{2\beta-1-\frac{n}{p}} \|u\|_{L^p(R^n)},$$

therefore, to make sure $\|u\|_{L^p(R^n)} = \|u_\lambda\|_{L^p(R^n)}$ to be true, we need $2\beta - 1 - \frac{n}{p} = 0$, that is $p = \frac{n}{2\beta - 1}$. So we have the proof done.

Then, we show the result that X is of the homogeneous Besov space $\dot{B}^s_{p,q}(R^n)$.

Theorem 2.2 Fractional Navier Stokes equations (1) are scaling invariant on $\dot{B}_{p,q}^{-(2\beta-1)+\frac{n}{p}}(R^n)$.

Proof: by the definition

$$\Delta_j u_\lambda(x) = \int_{R^n} \varphi_j(y) \lambda^{2\beta-1} u(\lambda(x-y)) dy$$
$$= \int_{R^n} \varphi_j(y) \lambda^{2\beta-1} u(\lambda x - \lambda y) dy,$$

taking the change of variable $\lambda y = y'$, that is $dy = \frac{1}{\lambda^n} dy'$, we have

$$\Delta_j u_\lambda(x) = \int_{R^n} \varphi_j(\frac{y'}{\lambda}) \lambda^{2\beta-1} u(\lambda x - y') dy'$$
$$= \lambda^{2\beta-1} \int_{R^n} \varphi_j(\frac{y'}{\lambda}) u(\lambda x - y') dy',$$

where

$$\varphi_j(\frac{y'}{\lambda}) = \int_{R^n} \phi(2^{-j}\xi) e^{2\pi i \frac{y'}{\lambda} \cdot \xi} d\xi = \int_{R^n} \phi(2^{-j}\lambda\xi') e^{2\pi i y' \cdot \xi'} \lambda^n d\xi'$$
$$= \lambda^n \int_{R^n} \phi(2^{-j}\lambda\xi') e^{2\pi i y' \cdot \xi'} d\xi',$$

where $\frac{\xi}{\lambda} = \xi'$, so we have

$$\varphi_j(\frac{y'}{\lambda}) = \lambda^n \int_{R^n} \phi(2^{-j}\lambda\xi') e^{2\pi i y' \cdot \xi'} d\xi',$$

Taking $2^{-j}\lambda = 2^{-j'}$, we get

$$j' = -\log_2 2^{-j\lambda} = -(\log_2 2^{-j} + \log_2 \lambda) = j - \log_2 \lambda.$$

Therefore, we obtain

$$\varphi_j(\frac{y'}{\lambda}) = \lambda^n \int_{R^n} \phi(2^{-j}\xi) e^{2\pi i y' \cdot \xi} d\xi = \lambda^n \varphi_{j'}(y'),$$

which implies $\Delta_j u_\lambda(x) = \lambda^{2\beta-1-n} \int_{R^n} \lambda^n \varphi_j(y') u(\lambda x - y') dy'$. As a result,

$$\|\Delta_j u_\lambda(x)\|_{L^p(R^n)} = \left(\int_{R^n} |\lambda^{2\beta-1} \int_{R^n} \varphi_{j'}(y') u(\lambda x - y') dy'|^p \, dx \right)^{\frac{1}{p}}$$
$$= \left(\int_{R^n} |\lambda^{2\beta-1} \int_{R^n} \varphi_{j'}(y) u(\lambda x - y) dy|^p \, dx \right)^{\frac{1}{p}}.$$

Taking a change of variable $\lambda x = x'$, that is hence $x = \frac{x'}{\lambda}, dx = \frac{1}{\lambda^n} dx'$, hence

$$\left\| \Delta_j u_\lambda(x) \right\|_{L^p(R^n)} = \left(\int_{R^n} | \lambda^{2\beta-1} \int_{R^n} \varphi_{j'}(y) u(x'-y) dy |^p \frac{1}{\lambda^n} dx' \right)^{\frac{1}{p}}$$

$$= \lambda^{2\beta-1-\frac{n}{p}} \left(\int_{R^n} | \int_{R^n} \varphi_{j'}(y) u(x'-y) dy |^p \, dx' \right)^{\frac{1}{p}} = \lambda^{2\beta-1-\frac{n}{p}} \left\| \Delta_{j'} u \right\|_{L^p(R^n)}.$$

By the definition of the norm of Besov spaces,

$$\| f \|_{\dot{B}^s_{p,q}(R^n)} = \left(\sum_{j=-\infty}^{\infty} (2^{sj} \left\| \Delta_j f \right\|_{L^p(R^n)})^q \right)^{\frac{1}{q}},$$

we have $\| f_\lambda \|_{\dot{B}^s_{p,q}(R^n)} = \left(\sum_{j=-\infty}^{\infty} (2^{sj} \left\| \Delta_j f_\lambda \right\|_{L^p(R^n)})^q \right)^{\frac{1}{q}}$, by the conclusion that

$$\left\| \Delta_j f_\lambda \right\|_{L^p(R^n)} = \lambda^{2\beta-1-\frac{n}{p}} \left\| \Delta_{j'} f \right\|_{L^p(R^n)},$$

where $j' = j - \log_2 \lambda$. Thus, the norm of u_λ in $\dot{B}^s_{p,q}(R^n)$ is

$$\| u_\lambda \|_{\dot{B}^s_{p,q}(R^n)} = \left(\sum_{j=-\infty}^{\infty} (2^{sj} \lambda^{2\beta-1-\frac{n}{p}} \left\| \Delta_{j'} u \right\|_{L^p(R^n)})^q \right)^{\frac{1}{q}}$$

$$= \left(\sum_{j=-\infty}^{\infty} (2^{sj'} \lambda^s \lambda^{2\beta-1-\frac{n}{p}} \left\| \Delta_{j'} u \right\|_{L^p(R^n)})^q \right)^{\frac{1}{q}}$$

$$= \lambda^{s+2\beta-1-\frac{n}{p}} \left(\sum_{j'=-\infty}^{\infty} (2^{sj'} \left\| \Delta_{j'} u \right\|_{L^p(R^n)})^q \right)^{\frac{1}{q}}$$

$$= \lambda^{s+2\beta-1-\frac{n}{p}} \| u \|_{\dot{B}^s_{p,q}(R^n)},$$

where we used $j = j' + \log_2 \lambda$ and $sj = sj' + s\log_2 \lambda$, therefore

$$2^{sj} = 2^{sj' + s\log_2 \lambda} = 2^{sj'} 2^{s\log_2 \lambda} = 2^{sj'} \lambda^s .$$

To make sure $\| u_\lambda \|_{\dot{B}^s_{p,q}(R^n)} = \| u \|_{\dot{B}^s_{p,q}(R^n)}$, we need

$$s + 2\beta - 1 - \frac{n}{p} = 0 \Rightarrow s = -(2\beta - 1) + \frac{n}{p}.$$

It follows that the homogeneous Besov space should be chosen as $\dot{B}^s_{p,q}(R^n) = \dot{B}^{-(2\beta-1)+\frac{n}{p}}_{p,q}(R^n)$. Consequently we have the proof done.

By the embedding theorem of the homogeneous Besov spaces, we know that when p, q are infinity, the space is the biggest one $\dot{B}^{-(2\beta-1)}_{\infty,\infty}(R^n)$. And if $\beta = 1$, the system (1) becomes Navier-Stokes equations, the corresponding scaling invariant space is $\dot{B}^{-1}_{\infty,\infty}(R^n)$. If $\beta = 0$, the system (1) correspond to Euler equations, then the corresponding scaling invariant space is $\dot{B}^{1}_{\infty,\infty}(R^n)$.

III. CONCLUSIONS

We consider the value of the index parameters p in Lebesgue spaces $L^p(R^n)$, and s, p, q in homogeneous Besov spaces $\dot{B}^s_{p,q}(R^n)$ for fractional Navier-Stokes equations to be scaling invariant in these spaces. We conclude that, the parameter p in Lebesgue spaces must be $p = \frac{n}{2\beta - 1}$, and the homogeneous Besov space must be $\dot{B}^{-(2\beta-1)+\frac{n}{p}}_{p,q}(R^n)$. Due to the embedding theorem in homogeneous spaces, we know for fractional Navier-Stokes equations the biggest scaling invariant homogeneous Besov space is $\dot{B}^{-(2\beta-1)}_{\infty,\infty}(R^n)$. And as the parameter special cases, we know the biggest s homogeneous Besov space for Navier-Stokes equations is $\dot{B}^{-1}_{\infty,\infty}(R^n)$, the one for Euler equations is $\dot{B}^{1}_{\infty,\infty}(R^n)$.

REFERENCES

[1] JL. Lions, "Quelques méthodes de résolution des problèmes aux limites non linéaires", (French), Paris: Dunod/Gauthier-Villars, 1969.

[2] J. Wu, "Generalized MHD equations, Journal of Differential equations", 195, 284-312, 2003.

[3] J. Wu, "The generalized incompressible Navier-Stokes equations in Besov spaces", Dynamics of PDE. 1, 381-400, 2004.

[4] J. Wu, "Lower bounds for an integral involving fractional Laplacians and the generalized Navier-Stokes equations in Besov spaces", Communications in Mathematical Physics, 263, 803-831, 2005.

[5] T. Runst, W. Sickel, "Sobolev spaces of fractional order, Nemytskij operators, and nonlinear partial differential equations", de Gruyter Series in Nonlinear Analysis and Applications, 3, Walter de Gruyter: Berlin, 1996.

[6] C. Miao, B. Yuan, B. Zhang, "Well-posedness of the Cauchy problem for the fractional power dissipative equations", Nonlinear Analysis: Theory, Methods & Applications, 68, 461–484, 2008.

[7] X. Yu, Z. Zhai, "Well-posedness for fractional Navier-Stokes equations in the largest critical spaces", Mathematical Methods in Applied Sciences, 35, 676–683, 2012.

[8] Z. Zhai, "Global well-posedness for nonlocal fractional Keller-Segel systems in critical Besov space", Nonlinear Analysis: Theory, Methods & Applications, 72, 3173–3189, 2010.

International Journal of Innovation Engineering and Science Research

Open Access

Performance Comparison of Power Control Methods That Use Neural Network and Fuzzy Inference System in CDMA

Yalcin Isik
Silifke-Tasucu Vocational High School, Selcuk University
Mersin, Turkey

ABSTRACT

In the cellular communication applications of Code Division Multiple Access (CDMA) system, each user signal can be received in the different power levels in the input of the base station due to different distances of the users. In that case, signal of the user that is closer to the base station increases the communication errors of the far users. To solve this problem, open or closed loop power control system is used to make each user signal equals in the input of the base station. Power prediction and power control have been performed with various methods in the literature. In this study, two different methods will be investigated and will be compared with each other in terms of power control performance. The power at the output of the matched filter is predicted using neural network and fuzzy inference system, power control is realized according to the predicted values.

Keywords—*CDMA; Power Control; Neural Network; Fuzzy Inference System*

I. INTRODUCTION

In a code division multiple access (CDMA) system, a number of users simultaneously transmit information over a common channel, each user`s signal is assigned a different signature waveform, and the received signal is the superposition of the signals transmitted by each user. In the receiver, user data is obtained by multiplying the received signal with its own spreading code. In the system, when the signal powers of the users are different, errors of the user data that has weak signal power increase; this situation is called as the near-far problem. The power controlsystem is used to overcome this problem. The power control system assures that all signal levels are the same in the input stage of the base station.

The power control is performed as open-loop or closed-loop. In the open-loop control, the power of the mobile user`s transmitter is adjusted by itself evaluating signal power that is transmitted from the base station. In this method, path losses are assumed as the same from the base station to mobile user and from the mobile user to the base station. However, open-loop control is not sufficient method, because these losses can not be the same in the real application. In the closed-loop control, base station detects the power level of the mobile user and transmits power control signal to the mobile user to adjust its power. In this way, all the mobile user`s signals are received in the base station with the same power level due to control signals that is transmitted from the base station system. However, determination of the signal power of each mobile user in the base station is not easy process, because all the user`s signals are combined as one CDMA signal. There are various studies about this subject in the literature, but generally they consist of complex structures. A FIR filter was used for prediction of the signal power in [1]. A predictive low pass filtering was used to improve power estimation in [2,3,4]. A fuzzy system was used to make power level estimation in [5]. However, an optimized neural network was used for power prediction in [6], and Elman neural network were used to control the power in [7] with the complex structures. Neural Network was used to predict the power from output of the matched filter in [9] and Fuzzy Inference System was used to predict the power from output of the matched filter in [10].

In this study, Neural Network (NN) and Fuzzy Inference System (FIS) will be compared in terms of power control performance in CDMA system. The power level prediction is realized with NN and FIS by evaluating outputs of the matched filters, and the closed-loop power control was used to adjust the power of the mobile user by small steps.

II. System Model

We consider synchronous CDMA system with binary phase shift keying (BPSK) modulation in an additive white Gaussian noise (AWGN) channel. Data for each user as random series in form of -1,+1 is generated and multiplied with its spreading code to obtain a CDMA signal. The CDMA signals of all users and AWGN are added in the channel. At the receiver, the received CDMA signal with the K users is multiplied with kth user signature waveform and integrated in one bit period to make an estimation for kth user bit. The output of the kth matched filter in one symbol interval yk is given by

$$y_k = A_k b_k + \sum_{\substack{j=1 \\ j \neq k}}^{K} A_j b_j \rho_{jk} + n_k \qquad (1)$$

where bk is the input bit of the kth user (desired user), bk∈{-1, +1}, bj is the input bit of the jth user, Ak is the received amplitude of the kth user, Aj is the received amplitude of the jth user, ρ_{jk} is the cross-correlation coefficient between desired user and the jth user, and nk is additive white Gaussian noise. The second term in Eq.(1) is the multiple access interference (MAI) that is effect of the other active users. In the base station, the power level of each user is determined with the output of the matched filter as:

$$p_k = \frac{1}{M} \sum_{j=1}^{M} (y_{k(j)})^2 \qquad (2)$$

Where pk is the power of the kth user, k is the user`s number and M is the number of the bits that are considered in the calculation of the power. The power estimation and the control are done with the outputs of the matched filters as in Fig. 1.

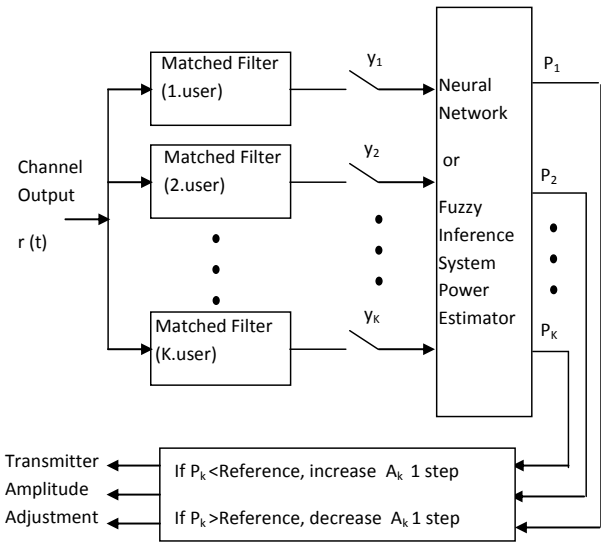

Fig. 1. The structure for the power estimation from the outputs of the matched filters and the control of the power level.

III. Artificial Neural Networks

The neural networks are constructed with neurons that connected to each other. Each connection has a weight factor and these weights are adjusted in a training process. There are many types of the neural networks for various applications in the literature. A common used one of these is the multilayered perceptrons (MLP) [8]. MLPs consist of input, hidden and output layers and they have feedforward connections between neurons. Neurons in the input layer only act as buffers for distributing the input signals to the neurons in the hidden layer. There are various activation functions that are used in the neurons. The weights are changed with various learning algorithm for getting proper output. The basic structure of the neural network with N input and one output is shown in Fig. 2. In this study, the Levenberg-Marquardt algorithm is used as the learning algorithm for the MLPs [8].

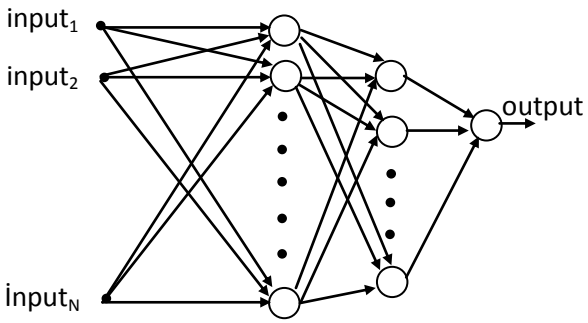

The basic structure of the neural network with N input, one output.

IV. Fuzzy Inference System

Fuzzy Inference System (FIS) constitute the outputs by evaluating the inputsaccording to the rules defined before.The structure of Fuzzy Inference System with r rules, n inputs and m outputs is shown in Fig. 2. Fuzzy inference process is made of 5 parts. Adjustment of the inputs variables to the fuzzy values, application of the fuzzy logic operands (AND or OR) to the adjusted values, obtaining the end values from the initial values, evaluating of the obtained values according to the rules, and back transformation from the fuzzy logic values.

In this study, Sugeno type FIS is used after the matched filter, the character of proper membership function for FIS is determined by calculating the power of an user in equation 2. In this receiver; Gaussian has been used for all of the input membership functions, triangle type has been used for output membership functions, and VE operator has been used between the inputs. Rules are set as depended on the power values which are calculated from equation 2 different power level matched filter output, and are depended on the number of user. For 3 users, 16 rules are being applied and for this reason 16 bit training data is sufficient. Output power for every user is determined according to these 16 rules. These rules can be determined for 2 different power levels like this:

$$\text{Rule(j): IF } y_{1j} \text{ and } y_{2j} \text{ and } \ldots\ldots\ldots y_{Kj} \text{ THENoutput}_k = P_i$$

where k=1,2,…,K (K number of users), j=1,2,…,J (J number of bit $J=2x2^K$), i=1 and 2, P consists of output power and different power levels used in training for user.

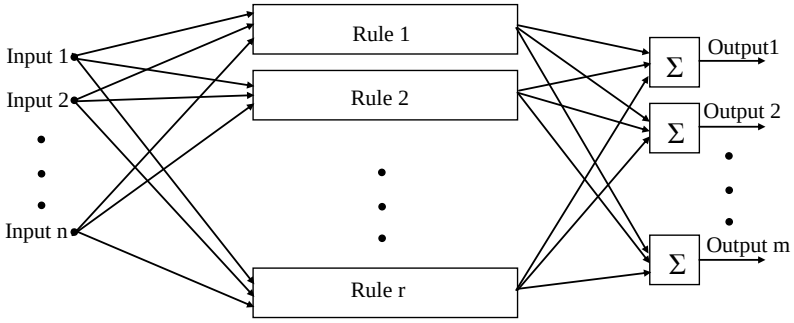

Fig. 2. The structure of Fuzzy Inference System with n inputs, r rules and m outputs.

V. SIMILATION RESULTS

In the simulation of the CDMA system, 31 bits length spreading codes that have normalized cross-correlation 0.2258 between each other were used. Cross-correlation value is selected bigger to create a more severe near-far environment. The simulations were done in the three users synchronous AWGN channel.

In the neural network that is used in the system, the number of the input and hidden layer nodes were chosen as the number of the users, and the number of output node was chosen as 1. The network is a feed forward network and it was trained by Levenberg-Marquardt algorithm. In the hidden layer tangent sigmoid activation function was used and in the output layer pure linear activation function was used. The power estimation and the control were done only for the first user that is selected as the desired user. The power control was performed to make the powers of the all users as 2 watt in the input of the base station. The powers of the second and the third users were assumed as 2 watt during the training and in the simulations. The training data that is produced for the three different power level as 1,2 and 3 watt were used during the training. The 8 bits training data that is all the possible combinations of three users were used without noise for each power level.

In the simulation, the performance of the power estimation and control of the neural network and fuzzy inference system was examined in the synchronous AWGN channel with 10 dB and 25 dB signal to noise ratios (SNR) of the first user. The SNR of the first user is defined as:

$$SNR_1 = \frac{signal\ power}{noise\ power} = \frac{A_1^2}{2\sigma^2} \qquad (3)$$

where σ2 is the variance of the Gaussian noise with the zero mean value, A1 is the amplitude of the first user`s signal and Ak is the amplitude of user k's signal. All the simulations were done for the three methods as mean of the squares of the output of the matched filter of the first user, the neural network and fuzzy inference system estimator. The powers of the second and the third user were assumed as 2 watt whereas the power of the first user was assumed as 1 watt at the beginning. The power control was performed to make the power of the first user 2 watt in the input of the base station. The amplitude of the first user was changed by the 0.1 steps depending on estimated power level. The results for the case that is considered 1 bit and 50 bits for each estimation are shown in Fig. 4 and Fig. 5, respectively, for 100 different estimation in the channel with 10 dB SNR value. As it is shown, the estimation performance of the neural network is better than mean squares method, and also fuzzy inference system is much better than neural network. Power control can be done between 0 watt-5 watt with mean squares, 1.5 watt-3 watt with neural network and 1.8 watt-2.8 watt with fuzzy inference system by considering 1 data bit for each estimation in the channel with 10 SNR value.Furthermore, in the case that is considered 50 bits for each estimation, power control performance gets better for all methods. Fuzzy inference system has still the best performance. A better estimation can be done by considering more values for the estimation, but in that case estimation time increases.

Furthermore, the case that is considered 50 bits for each estimationin the channel with 25 dB SNR value is shown in Fig. 6.As it is shown, the power control depends on neural network and fuzzy inference system estimator can be performed very good especially for the bigger SNR values.Fuzzy inference system has the best performance again.

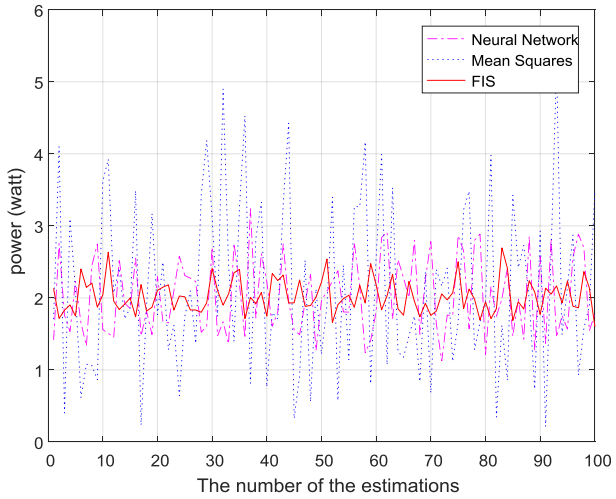

Fig. 3. The power control performance considering 1 bit data foreach estimation in the channel with 10 dB SNR value.

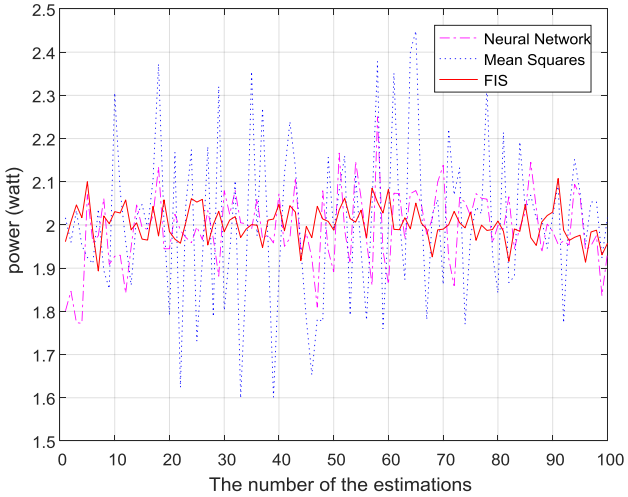

Fig. 4. The power control performance considering 50 bit data foreach estimation in the channel with 10 dB SNR value.

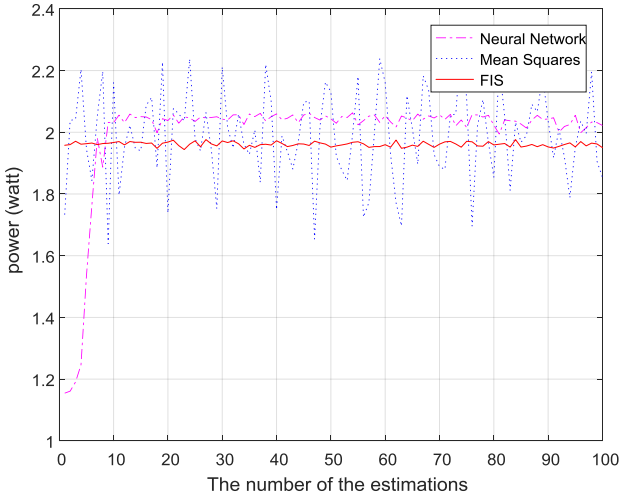

Fig. 5. The power control performance considering 50 bit data foreach estimation in the channel with 25 dB SNR value.

VI. Conclusion

The power level can be defined by calculating mean-squares of the values that are taken from the output of the matched filter. However, the number of the considered values for the calculation of the power level must be high to get more correct power level. But considering more values causes slow power control. The power control must be fast enough for the effective communication. Simulations results show that the fast power control can be performed with NN and FIS approach even in 1 bit period. However, the estimation performance of the Fuzzy Inference System is better than Neural Network. Performances of the NN and FIS estimators get better for the bigger SNR values. A better power estimation can be done by considering more values for the estimation, but in that case estimation time increases.

References

[1] J.M.A. Tanskanen, A. Huang, T.I. Laakso,S.J.Ovaska, "Prediction of received signal power in CDMA cellular systems," Proc. of 45th IEEE Vehicular Technology , Chicago, Illinois,pp. 922–926, 1995.

[2] J.M.A. Tanskanen, A. Huang, I.O.Hartimo," Predictive power estimators in CDMA closed loop power control," Proc. of 48th IEEE Vehicular Technology Conference, Ottawa, Ontario, Kanada, pp. 1091–1095, 1998.

[3] J.M.A. Tanskanen, J. Mattila, M. Hall,T. Korhonen,S.J. Ovaska, "Predictive closed loop power control for mobile CDMA systems," Proc. of 47th IEEE Vehicular Technology Conference, Phoenix, Arizona, USA, pp. 934–938, 1997.

[4] J.M.A. Tanskanen, J. Mattila, M. Hall,T. Korhonen,S.J. Ovaska,."Predictive closed loop transmitter power control," Proc. of 1996 IEEE Nordic Signal Processing Symposium, Espoo, Finland, pp. 5–8, 1996.

[5] P.R. Chang, B.C. Wang, "Adaptive fuzzy proportional integral power control for a cellular CDMA system with time delay," IEEE Journal on Selected Areas in Communications, Vol.14 (9), pp. 1818-1829, 1996.

[6] X.M. Gao, X.Z. Gao, J.M.A. Tanskanen, S.J. Ovaska, "Power prediction in mobile communication systems using an optimal Neural-Network Structure," IEEE Transactıons on Neural Networks, Vol.8 (6), pp. 1446-1455, 1997.

[7] X.Z. Gao, S.J. Ovaska, A.V. Vasilakos, "A modified Elman neural network based power controller in mobile communications systems," Soft Computing, Vol.9, pp. 88-93, 2005.

[8] M.T. Hagan, H.B. Demuth, M. Beale M, Neural network design, PWS Publishing Company 1996

[9] Y. Işık,N. Taşpınar, "Power control by using Neural Network in the synchronous CDMA systems," The 14. Turkish symposium on Artificial Intelligence and Neural Networks (TAINN'2005), İzmir, pp. 393-399, June 16-17, 2005.

[10] Y. Işık,N. Taşpınar,"Power control by using Fuzzy Inference System in the CDMA systems,"URSI-Turkey, pp. 470-472, 8-10 September 2004.